AMPLIFICATION CRITERION OF GRADUALLY VARIED, SINGLE PEAKED WAVES

by

JOHN PETER JOLLY and VUJICA YEVJEVICH

December 1971

HYDROLOGY PAPERS
COLORADO STATE UNIVERSITY
Fort Collins, Colorado

51

AMPLIFICATION CRITERION OF GRADUALLY VARIED, SINGLE PEAKED WAVES

by

John Peter Jolly* and Vujica Yevjevich**

HYDROLOGY PAPERS
COLORADO STATE UNIVERSITY
FORT COLLINS, COLORADO 80521

December 1971

No. 51

*Assistant Professor, Department of Civil Engineering, Faculty of Science and Engineering, University of Ottawa, Ottawa, Canada.

**Professor of Civil Engineering, Colorado State University, Fort Collins, Colorado.

TABLE OF CONTENTS

LIST OF FIGURES

LIST OF FIGURES (continued)

LIST OF FIGURES (continued)

LIST OF SYMBOLS

Symbol	Definition
a	Coefficient in frictional law
A	Cross-sectional area-ft^2
A_H	Acceleration parallel to channel bed-ft/sec^2
A_V	Acceleration normal to channel bed-ft/sec^2
b	Exponential coefficient in frictional law
B	Base width-ft
C	Chezy resistance constant
C_5	Frictional law constant
C_6	Frictional law constant
d	Cross-sectional shape factor
f	Frictional factor
F	Froude number – $V/\sqrt{gy}$
F_b	Froude number of base flow
F_P	Froude number of wave peak
F_s	Stability Froude number
g	Accelerations due to gravity – 32.2 ft/sec^2
k	Roughness height
K	f/8g
L	Reference for integration technique
m	Subscript representing maximum depth at any x
P	Wetted perimeter – ft
q	Lateral discharge – ft^3/sec/ft
Q	Discharge – ft^3/sec

Symbol	Definition
R	Hydraulic radius – ft
Re	Reynolds number – VR/ν
S_f	Frictional slope
S_o	Bed slope
t	Time – sec
v	Velocity of water particle - ft/sec
V	Average velocity – ft/sec
V_f	Velocity on wave front – ft/sec
V_o	Uniform flow velocity –ft/sec
V_r	Velocity on wave rear – ft/sec
x	Distance – ft
y	Depth – ft
y_b	Base depth – ft
y_o	Uniform flow depth – ft
ϵ^+	Slope of positive characteristic
ϵ^-	Slope of negative characteristic
λ	Peak parameter of inflow hydrograph
θ	Skewness parameter of inflow hydrograph
ν	Kinematic viscosity
ρ	Mass density
υ	Vedernikov number
υ_b	Vedernikov number of base flow
υ_p	Vedernikov number at wave peak

ACKNOWLEDGMENT

This paper is based on the Ph.D. dissertation submitted and defended by J. P. Jolly, and guided and advised by Dr. V. Yevjevich, the major professor and chairman of the Ph.D. committee. Acknowledgment goes also to Dr. Albert H. Barnes, Associate Professor of Civil Engineering at Colorado State University, for his advice and cooperation, as well as to other members of the Ph.D. committee.

Acknowledgments also go to the U.S. Federal Highway Administration, previously the U.S. Bureau of Public Roads, for their support of the project "Unsteady Free Surface Flow in a Storm Drain," from which some materials have been used, and to the Computer Centre of the University of Ottawa, Ottawa, Canada, where the simulations were made.

The Department of Civil Engineering of the University of Ottawa, Ottawa, Canada, and the Department of Civil Engineering of Colorado State University, Fort Collins, Colorado, U.S.A., have given all necessary help and encouragement for completion of this study. Both writers gratefully appreciate the support of these institutions.

ABSTRACT

Some hydraulic properties, obtained using the Chézy resistance law, that distinguish amplifying waves from attenuating waves are found by a numerical integration of the governing hyperbolic, partial differential equations of supercritical, gradually varied waves flowing in a channel with a rectangular cross section. The supercritical, gradually varied flow is simulated by using various integration techniques of the specified intervals scheme of the method of characteristics solution to the governing system of equations. One of these integration techniques is used to determine attenuation and amplification characteristics of gradually varied, single peaked waves. Prior to this determination, criteria found by various investigators for predicting the stability of uniform flow are shown to be equivalent. One of the criteria, the Vedernikov number, which contains parameters dependent on the frictional law, channel cross-sectional shape and Froude number, is also the criterion for predicting amplification of gradually varied, single peaked waves.

Chapter 1

INTRODUCTION

In most natural and artificially constructed streams, once a flood wave is initiated it will attenuate as it travels along a channel. In some streams or along spillways, and in many storm culverts, however, the flow may become supercritical; and if the Froude number ($F = V/\sqrt{gy}$) is above a certain value, the peak depth will increase with distance along the channel. These increases in flow depth can cause excessive hydrodynamic pressures to come to bear against hydraulic structures, as in the case of a tailrace structure of a hydroelectric station in the USSR as related by Ghambarian (1965); or cause the flow to overtop the banks of channels with steep bed slopes, as is the case of an irrigation canal in Los Angeles – Brock (1967). A criterion or criteria have not, as yet, been developed to determine whether or not these supercritical waves will grow in height along a channel.

Instability in open channel flow is defined as flow conditions that result when the peak depth of flow or peak value of any other parameter increases with distance along the channel. In steady flow, the water surface profile develops into a series of roll waves that increase in depth at the crests and decrease in depth at the troughs as it travels down the channel. This is normally referred to as roll waves, and represents instability of steady flow. With unsteady, single peaked waves instability occurs when the peak depth of the wave increases with the distance along the channel. This instability has been often observed in nature in open channels (Blair, Cornish, and Holmes) and normally is referred to as the passage of gradually varied waves to slug flow.

Unsteady flow may either be gradually varied or rapidly varied. The equations governing the gradually varied flow are one-dimensional. For this flow it is assumed that the vertical accelerations are small compared with the total accelerations. With rapidly varied flow the governing equations are two-dimensional, and the vertical accelerations along the channel are large when compared with the accelerations parallel to the channel bed.

During the past century, numerous engineers and mathematicians have developed criteria for determining the stability of open channel flow for a uniform regime but not for unsteady flow. In general, these criteria give the Froude number above which uniform flow ($\frac{\partial y}{\partial x} = 0$, $\frac{\partial y}{\partial t} = 0$) becomes unstable for a particular geometry of the cross-sectional area and the resistance law of flow. These efforts have been culminated with the work of Vedernikov, Iwasa, Craya, Keulegan and Patterson, each developing the same criterion, but by different methods.

Until 1960 all experiments in open channel flow hydraulics were conducted either in the laboratory under controlled conditions or in the field. The types of flow observed were classified as steady or unsteady and either uniform, gradually varied, or rapidly varied. Mathematical equations have been derived to describe these various types of flow – see bibliography on unsteady flow by Yevjevich (1964). The solution of these equations represents the flow that would occur in a physical state. The available solutions of these equations, however, were limited to simplified conditions such as the bed slope and frictional resistance being equal to zero. Fortunately during the 1960's methods and techniques became available for simulating gradually varied flow by the numerical integration of the governing equations on a digital computer, thereby providing an alternate to the physical experiments.

In both cases, physical and numerical experiments, there are always errors. In a physical experiment there are errors resulting from the specification tolerances of the boundary and the initial conditions and in the means of measuring the flow parameters. In a numerical experiment, or simulation, although the boundary and initial conditions can be prescribed with precision, there still remains both truncation errors in the computations, errors in the written output, as well as errors resulting from the finite difference approximations to the mathematical derivatives and in the integration of the partial differential equations.

Using the work by Yevjevich and Barnes (1970) and Zovne (1970) on the numerical solution as a point of departure, it is the objective of this paper to determine the criterion or criteria for instability of gradually varied, single peaked waves. These criteria are determined by numerical simulations, which are

assumed to be sufficiently accurate and far less expensive to arrive at than from physical experiments. Moreover, it is questionable whether measuring techniques are yet available to accurately determine, both spatially and temporally, the depths and velocities simultaneously of flows with high Froude numbers. To describe these stability phenomena certain terms have been used in the past. In the work on uniform flow regimes, the development of roll waves has been referred to as free surface instability (Koloseus and Davidson) or as instability (Iwasa). The only analytical work so far on the same type of problem in supercritical, gradually varied flow (Zovne) also uses the terms stability and instability. Both Zovne and the writers have used the numerical solution on the gradually varied flow equations in studying waves in supercritical regime. The solution of these equations can be numerically unstable under certain conditions when the flow is stable. Therefore, the writers will not use the term stability as used in the hydraulic sense when discussing gradually varied flow. Rather, when the peak depths of gradually varied, single peaked waves become smaller as the waves travel along a channel, they are said to be attenuating; when the peak depths become larger as the waves travel along a channel, they are said to be amplifying. When discussing other works with uniform flow, however, the term stability will be used. Therefore, what is being considered is the criterion or criteria for amplification of a wave travelling along a channel whose slope is supercritical with respect to the base flow discharge of the hydrograph. In other words, the amplification of a single peaked, supercritical wave, which is governed by the equations of gradually varied flow, is studied with respect to finding criterion or criteria for amplification.

Chapter 2

LITERATURE REVIEW

There have been at least three occasions when amplifying waves have been observed in nature and recorded in the literature. Cornish (1934) was the first to mention that the peak depth of supercritical flow in open channels could amplify. By observing the flow in drainage channels in the Swiss Alpes, he noticed that a series of roll waves formed which grew in height as they travelled along a channel.

Two years later Holmes (1936), standing on a bridge over one of the flood control channels in Los Angeles, observed over an interval of several minutes that the flow depth increased from approximately three feet to approximately eight feet and then subsided to three feet. This was followed by another wave of larger amplitude which also subsided to the original flow depth. Blair (1961) reported,that on the Nisqually River in the State of Washington in October 1955 that two National Park Rangers observed five or six surges over a duration of 45 minutes which were 15 to 20 feet higher than the water level immediately in front of the surges. The first surge washed away a highway bridge that had had 40 feet clearance above the alluvial bed.

There has been no detailed experimental or theoretical work published that explains why the flow conditions cited above do occur in nature. Moreover, all analytical and experimental studies of amplification in the supercritical regime have been limited to supercritical, uniform flow with the exception of Zovne's work with supercritical, non-uniform flow which will be discussed later.

A review of some of the analytical work on stability criteria for uniform flow is as follows.

Keulegan and Patterson (1940) determined a stability criterion mathematically from Boussinesq's equation for the velocity of propagation of a volume element of a wave and an equation relating frictional resistance with depth for supercritical, uniform flow. They determined that instability will occur when the gravitational force is greater than the frictional force. Their stability criterion is

$$\rho g y S_o - \frac{f\rho V^2}{8} \quad \begin{bmatrix}\text{unstable}\\ \text{stable}\end{bmatrix} \quad \begin{matrix}>\\<\end{matrix} \quad 0 , \qquad (2.1)$$

or in terms of slopes in dividing Equation 2.1 by $\rho g y$ it can be expressed as

$$S_o - S_f \quad \begin{bmatrix}\text{unstable}\\ \text{stable}\end{bmatrix} \quad \begin{matrix}>\\<\end{matrix} \quad 0 . \qquad (2.2)$$

In Equations 2.1 and 2.2, ρ is the fluid density, g is the acceleration due to gravity, y is the flow depth, S_o is the bed slope, f is the frictional factor, V is the flow velocity, and S_f is the frictional slope.

Also, Vedernikov (1945) determined a stability criterion by using the equations of gradually varied flow and by considering the time growth or decay of energy of a small disturbance on a steady, uniform flow. His criterion is

$$\upsilon = \left(\frac{1 - b}{2 + b}\right) \left(1 - R\frac{dP}{dA}\right) F \qquad (2.3)$$

in which υ is the Vedernikov number, b is the exponential coefficient in the resistance law $f = a(Re)^b$ for a hydraulically smooth conduit, R is the hydraulic radius, P is the wetted perimeter, A is the cross-sectional area, F is the Froude number and a is a coefficient. When $\upsilon > 1$ the flow is unstable; when $\upsilon = 1$ the flow is neutrally stable; and when $\upsilon < 1$ the flow is stable.

Craya (1952) considered steady flow near normal depth thereby eliminating the terms in the gradually varied flow equations that vary with time; thus the partial derivatives become total derivatives. He showed that the flow would become unstable when the Seddon* celerity, dQ/dA , is greater than the Lagrangian celerity, $V + \sqrt{gy}$, *i.e.*,

$$dQ/dA > V + \sqrt{gy} \qquad (2.4)$$

Iwasa (1954) considered the initiation of continuous time growth of an infinitesimally disturbed wave. His criterion for flow with uniform velocity distribution is as follows.

*This celerity is known in the literature under the name Seddon, or Kleitz-Seddon, though the first author to obtain it was Graeff (1875) before Kleitz (1877) and Seddon (1900).

$$\frac{V}{\sqrt{\frac{gA}{dA/dy}}} = F_S \gtrless \frac{R\,\frac{dA}{dy}}{\frac{AdR}{dy}\left(\frac{3}{2} \times 0.4343\ C_5 f^{1/2} + 0.5\right)} \qquad (2.5)$$

in which f is given as

$$f = \frac{1}{[C_5 \log\ (\frac{4R}{k}\ C_6)]^2},$$

k is the height of the resistance roughness, C_5 and C_6 are constants.

Iwasa's criterion reduces to Vedernikov's for compatible conditions.

Koloseus and Davidson (1966), with uniform flows developed in a 3.0 foot wide and 85 foot long flume, obtained good correlation between the stability criterion of Keulegan and Patterson and the development of roll waves. They defined "roll waves" as any wave of spontaneous origin, regardless of size or shape, that is attributable to no cause other than the superiority of the gravitational force over the boundary retarding force. Although the work by Koloseus and Davidson is interesting but limited to depths near normal depth, it is shown in the next chapter that the criteria of Vedernikov, Keulegan and Patterson, and Craya, although expressed in different terms, are equivalent.

One investigator who did not limit his work to supercritical, uniform flow was Zovne (1970). Using a digital computer he compared simulated, gradually varied flows in the supercritical regime with two numerical schemes. He simulated the flows with both the characteristic grid scheme and specified intervals scheme of the method of characteristics and showed that each method gives almost identical results. Both the characteristic grid and specified interval schemes are ways in which the equations of gradually varied flow may be solved by the method of characteristics.

He also simulated with the specified intervals scheme an experiment in a flume where the raising of a tailgate caused a hydraulic jump to move upstream. In his simulations a sequential depth relation was used, and the wave profiles were not determined at the jump. The experimentally determined and numerically simulated positions of the physical jumps were compared as they moved upstream. Zovne's work provides proof that supercritical, gradually varied flow can be simulated with the method of characteristics. Some of his results are discussed in Chapter 4.

Chapter 3

THEORETICAL CONSIDERATIONS

3.1 Uniform Flow

In the previous chapter it was stated that the stability criteria developed by Keulegan and Patterson, and then by Vedernikov and later by Craya are one and the same. To understand this, the work by Keulegan and Patterson should be considered in terms of gravitational and frictional slopes, *i.e.*, instability will occur when $S_o > S_f$. Craya states, moreover, that instability will occur when the Seddon celerity is greater than the Lagrangian celerity. The Seddon celerity represents the speed of travel of a small wave that has stabilized at an invariant form and is governed by channel resistance. The Lagrangian celerity represents the speed of travel of a very small wave under the exclusive actions of inertia and gravity. Since the Seddon celerity is inversely related to the frictional slope, one may state that $dQ/dA \gtrless V + \sqrt{gy}$ is equivalent to $S_o \gtrless S_f$.

Consider again the celerity relation for instability $dQ/dA > V + \sqrt{gy}$, in a prismatic channel such that $y = A/B$, and $A/PR = 1$, $V = KR^{\left[\frac{1-b}{2+b}\right]}$ in which $K = \frac{f}{8g}$ and $f=a(R_e)^b$. The Seddon celerity dQ/dA may be expressed as

$$V + A\frac{dV}{dA} , \qquad (3.1)$$

and by differentiating the expression for velocity with respect to area

$$\frac{dV}{dA} = K\frac{(1-b)}{(2+b)} R^{-\frac{1+2b}{2+b}} \frac{dR}{dA} . \qquad (3.2)$$

Now dR/dA may be expressed as

$$\frac{d(A/P)}{dA} = \frac{1}{P} - \frac{A}{P^2}\frac{dP}{dA} = \frac{1}{P}\left(1 - R\frac{dP}{dA}\right). \qquad (3.3)$$

Therefore

$$\frac{dQ}{dA} = V + V\left(\frac{1-b}{2+b}\right)\frac{A}{PR}\left(1 - R\frac{dP}{dA}\right) . \qquad (3.4)$$

Equation 3.4 becomes

$$\frac{dQ}{dA} = V + V\left(\frac{1-b}{2+b}\right)\left(1 - R\frac{dP}{dA}\right) . \qquad (3.5)$$

The criterion for unstable conditions may be expressed by

$$V\left(\frac{1-b}{2+b}\right)\left(1 - R\frac{dP}{dA}\right) > \sqrt{\frac{gA}{B}} ,$$

or

$$\frac{V}{\sqrt{\frac{gA}{B}}} > \frac{1}{\left(\frac{1-b}{2+b}\right)\left(1 - R\frac{dP}{dA}\right)} . \qquad (3.6)$$

The left side of Equation 3.6 is by definition the Froude number, F ; therefore, the criterion may be rewritten in the form

$$F = \frac{1}{\left(\frac{1-b}{2+b}\right)\left(1 - R\frac{dP}{dA}\right)} . \qquad (3.7)$$

The Verdernikov number is defined by Equation 2.3, or

$$\upsilon = \left(\frac{1-b}{2+b}\right)\left(1 - R\frac{dP}{dA}\right) F$$

which is identical to Equation 3.7, thus the criteria of slopes – Equation 2.2, Verdernikov number – Equation 2.3, and celerities – Equation 2.4, are one and the same.

3.2 Mathematical Development of Gradually Varied Flow Equations

The equations of gradually varied flow, known as the Barré de Saint-Venant equations, are equations of conservation of mass and conservation of linear momentum or

$$A\frac{dV}{dx} + V\frac{dA}{dx} + \frac{dA}{dt} - q = 0 , \qquad (3.8)$$

as the conservation of mass, and

$$\alpha V \frac{dV}{dx} + \beta \frac{dV}{dt} + g \frac{dy}{dx} = g(S_o - S_f) - \frac{\beta V q}{A}, \quad (3.9)$$

as the conservation of linear momentum,in which

$$\alpha = \frac{1}{AV^3} \int \int_A v^3 \, dA \quad (3.10)$$

and

$$\beta = \frac{1}{AV^2} \int \int_A v^2 \, dA \quad . \quad (3.11)$$

In the latter two equations v is the velocity at a point in the cross section.

These velocity coefficients, Equations 3.10 and 3.11, depend on the velocity distribution in a cross sectional area of flow. It is assumed in this study that the velocity distribution is uniform; therefore, $\alpha = \beta = 1$. Neither the lateral inflow nor outflow discharge, q , are considered in this study.

Because of the assumed uniform velocity distribution and because lateral inflow or outflow are not considered, the above equations simplify to

$$A \frac{dV}{dx} + V \frac{dA}{dx} + \frac{dA}{dt} = 0 \quad (3.12)$$

and

$$\frac{V}{g} \frac{dV}{dx} + \frac{1}{g} \frac{dV}{dt} + \frac{dy}{dx} = S_o - S_f \quad . \quad (3.13)$$

In using Equations 3.12 and 3.13 to model physical flow, the following assumptions are made.

(1) Vertical accelerations are negligible.

(2) The channel bed slope is mild enough so that $\tan\alpha = \sin\alpha$.

(3) The frictional slope, S_f, can be represented by the Darcy-Weisbach relation $h_f = fLV^2/2gdR$ in which f is the friction factor as a function of Reynolds number of the flow and it is assumed to be the same value for unsteady flow as for steady flow, and d is a shape factor.

(4) The pressure throughout the flow domain is hydrostatic.

The third assumption is sufficient but not necessary. Any mathematical relationship for frictional slope or any relation that equates it to a constant value will suffice. Moreover, in this study the Chézy resistance law is used. The following shows the relationship between the Chézy and Darcy-Weisbach relations.

The Chézy resistance law relates flow velocity to hydraulic radius and the frictional slope. It may be stated as $V = C\sqrt{RS_f}$ in which C is the Chézy constant. The Darcy-Weisbach resistance states that $S_f = f V^2/2gdR$ in which d is a constant that is dependent only on the cross-sectional shape. For circular sections d is equal to four, and for very wide rectangular cross sections d is equal to one. Other cross-sectional shapes have intermediate values of d . The frictional factor, f , is related to Reynolds number by $f = a(R_e)^b$ in which $R_e = Vy/\nu$, in which ν is kinematic viscosity. Thus, the Darcy-Weisbach relation may be written as

$$S_f = \frac{a V^{2+b}}{2g \, d\nu^b R^{1-b}} \, ,$$

and the Chézy relation as

$$S_f = \frac{V^2}{C^2 R} \quad .$$

The two relations are the same when $b = 0$ and $C = \sqrt{2gd\nu/a}$, which is a constant for given conditions of fluid, temperature, cross-sectional shape and roughness.

The equations of unsteady free-surface flow, Equations 3.12 and 3.13, form a system of quasi-linear, partial hyperbolic differential equations of the first order. Various possible methods for integrating these two partial differential equations are reviewed in references abstracted by Yevjevich (1964). One of these methods is the method of characteristics which was shown by Zovne (1970) to be applicable for supercritical flow. It was developed by Massau (1889) for integrating the two partial differential equations of unsteady flow in channels by a graphical procedure. This method has been also widely used for the solution of a variety of problems in physics and mechanics, and its detailed description can be found in Courant and Freidrichs (1948), Crandall (1956), and Streeter and Wylie (1967).

The solution of a specific problem by the method of characteristics using hand calculation, or graphical means, or desk calculators is extremely laborious and time consuming. As a result in the interval between 1889 and the advent of electronic computers, a variety of schemes for solving open channel flow problems by this method was

proposed. The details of these various schemes can be found in references abstracted by Yevjevich (1964). In general, solutions by the method of characteristics may be performed in two ways: by the graphical method and by the use of digital computers. Of the two, digital computer provides several advantages. A digital computer can not only do the tedious computations that are required for the graphical method, but it can also give the solution for the complete system of equations to a better degree of accuracy and precision.

In both procedures the method of characteristics uses the equations of continuity and momentum of unsteady flow, (3.12) and (3.13), along with the total differentials of the dependent variables, velocity and depth, which constitute four characteristic equations. By considering only prismatic channels – those of unvarying cross-sectional areas and constant bed slopes – then the cross-sectional area may be described by $A = By$ where y is the hydraulic depth. Thus, the characteristic equations are

$$\frac{A}{VB}\frac{\partial V}{\partial x} + \frac{\partial y}{\partial x} + \frac{1}{V}\frac{\partial y}{\partial t} = 0 \quad , \qquad (3.14)$$

$$\frac{V}{g}\frac{\partial V}{\partial x} + \frac{1}{g}\frac{\partial V}{\partial t} + \frac{\partial y}{\partial x} = S_o - S_f \quad , \qquad (3.15)$$

$$dV = \frac{\partial V}{\partial x}\,dx + \frac{\partial y}{\partial t}\,dt, \qquad (3.16)$$

and

$$dy = \frac{\partial y}{\partial x}\,dx + \frac{\partial y}{\partial t}\,dt \quad . \qquad (3.17)$$

The partial derivatives of y and V with respect to x and t are unknown, therefore, there are four equations and four unknowns. A method is now described that shows how the four equations are solved simultaneously for V and y at any x and t. The four equations can be expressed in the matrix equation:

$$\begin{bmatrix} \frac{A}{VB} & 0 & 1 & \frac{1}{V} \\ \frac{V}{g} & \frac{1}{g} & 1 & 0 \\ dx & dt & 0 & 0 \\ 0 & 0 & dx & dt \end{bmatrix} \begin{bmatrix} \frac{\partial V}{\partial x} \\ \frac{\partial V}{\partial t} \\ \frac{\partial y}{\partial x} \\ \frac{\partial y}{\partial t} \end{bmatrix} = \begin{bmatrix} 0 \\ S_o - S_f \\ dV \\ dy \end{bmatrix} \qquad (3.18)$$

This equation may be expressed in the format of matrix algebra as: [M] x [Z] = [N] , in which [M] is the coefficient matrix, and [Z] and [N] are vectors representing the unknown partial derivatives and the right side of the equation, respectively.

To obtain a solution of V and y at any x and t from this equation, let ΔM be the determinant of a matrix [M] and let ΔK_i represent a matrix formed by replacing a column (i) in [M] by [N] . From matrix algebra it may be proved that $Z_i = \Delta K_i / \Delta M$. The rows of [M] are linearly dependent, *i.e.*, there is an interdependency between the values of y and the values of V at any x and t.To satisfy this interdependency the determinant of the coefficient matrix ΔM must be equal to zero. Here the equation [M] [Z] = [N] becomes indeterminate and the values of $\frac{\partial V}{\partial x}, \frac{\partial V}{\partial t}, \frac{\partial y}{\partial x}$ and $\frac{\partial y}{\partial t}$ are not uniquely determined, *i.e.*, $z_i = \Delta K_i / \Delta M = 0/0$. Therefore, since the derivative must be finite in the flow phenomenon considered, ΔK_i must equal zero whenever ΔM equals zero.

By expanding the determinant of [M] and equating it to zero, a quadratic equation in dt/dx is obtained. Solving for both positive and negative values of dt/dx the following is obtained

$$\left(\frac{dt}{dx}\right)_+ = \frac{1}{V + \sqrt{Ag/B}} = \epsilon_+ \qquad (3.19)$$

and

$$\left(\frac{dt}{dx}\right)_- = \frac{1}{V - \sqrt{Ag/B}} = \epsilon_- \quad . \qquad (3.20)$$

The curves in the distance-time plane on which $\Delta M = 0$ are called the characteristics curves. On each, the value of dt/dx is a constant.

By expanding the determinant of any of the four ΔK_i in Equation 3.18 and setting it equal to zero, four different but equivalent partial differential equations are obtained of the type shown in the following equation.

$$\left\{\left[\frac{A}{VB}-\frac{V}{g}\right]\frac{dt}{dx}+\frac{1}{g}\right\}\frac{dy}{dx}+\frac{A}{VBg}\frac{dV}{dx}+$$

$$\frac{A}{VB}(S_o-S_f)\frac{dt}{dx}=0. \qquad (3.21)$$

Substituting the values of $\epsilon\pm$ from Equation 3.19 and 3.20 to Equation 3.21 the following ordinary differential equations in V and y are obtained:

$$\left\{\left[\frac{A}{VB}-\frac{V}{g}\right]\epsilon_+ + \frac{1}{g}\right\}\frac{dy}{dx}+\frac{A}{VBg}\frac{dV}{dx}+$$

$$\frac{A}{VB}(S_o-S_f)\,\epsilon_+=0, \qquad (3.22)$$

$$\left\{\left[\frac{A}{VB}-\frac{V}{g}\right]\epsilon_- + \frac{1}{g}\right\}\frac{dy}{dx}+\frac{A}{VBg}\frac{dV}{dx}+$$

$$\frac{A}{VB}(S_o-S_f)\,\epsilon_-=0, \qquad (3.23)$$

along the positive and negative characteristics, respectively.

To numerically integrate the above equations in order to determine the depth, y , and velocity, V , at any distance, x , and time, t , in a channel there are many schemes. Two of them are described in the next chapter. To reiterate both are schemes of a class of solution known as the method of characteristics. One is called the characteristic grid scheme; the other is called the specified intervals scheme.

Chapter 4

NUMERICAL SOLUTIONS OF GRADUALLY VARIED FLOW EQUATIONS

4.1 Introduction

In part 3.2 of Chapter 3, in which the mathematical equations of gradually varied flow were discussed in terms of the characteristic equations, both the characteristic grid and the specified intervals schemes of integrating the equations were mentioned. There are many other methods available by which these equations can be integrated, such as the Lax-Wendoff and the diffusing schemes. A survey of the available methods with a discussion of their advantages and limitations for the numerical integrations of the gradually varied flow equations may be found in a recent publication by Yevjevich and Barnes (1970). These investigators recommended the use of the method of characteristic over any other method. The two schemes of the method of characteristics are described in the following paragraphs.

4.2 Characterisitic Grid Scheme

The pair of first-order equations that represent the flow, Equations 3.22 and 3.23, of the previous chapter, have two real roots, $(\frac{dt}{dx})_+ = \epsilon_+$ and $(\frac{dt}{dx})_- = \epsilon_-$. A curve that at each of its points has the slope $(\frac{dt}{dx})_+$ is called a positive characteristic. A curve that at each of its points has the slope $(\frac{dt}{dx})_-$ is called a negative characteristic. There are, therefore, two families of intersecting curves that fill out the domain of the independent variables x and t. Typical patterns of intersecting characteristics for subcritical and supercritical flows are shown in Figure 4.1.

By a simultaneous solution of Equations 3.19, 3.20, 3.22, and 3.23, the depths and velocities of the flow may be determined at the points where the positive and negative characteristics intersect. They are found by integrating from two grid points where y and V are known, points R and S, to the third point, P which is the intersection of the characteristics that pass through points R and S shown schematically in Figure 4.2. To obtain y and V at point P after knowing their values at points R and S the equations resulting from the simultaneous solutions of Equations 3.19, 3.20, 3.22 and 3.23 are solved in a sequential order. These equations are:

$$t_P = \frac{x_S - x_R + t_R(V_R + \sqrt{gy_R}) - t_S(V_S - \sqrt{gy_S})}{V_R + \sqrt{gy_R} - V_S + \sqrt{gy_S}} \quad (4.1)$$

$$x_P = x_R + (V_R + \sqrt{gy_R})(t_p - t_R) , \quad (4.2)$$

$$y_P = \frac{V_R - V_S + \sqrt{gy_R} + \sqrt{gy_S} - g(S_R - S_o)(t_P - t_R) + g(S_S - S_o)(t_P - t_S)}{\sqrt{\frac{g}{y_R}} + \sqrt{\frac{g}{y_S}}} \quad (4.3)$$

and

$$V_P = V_R - \sqrt{\frac{g}{y_R}}\,(y_P - y_R) - g(S_R - S_o)(t_P - t_R) \quad (4.4)$$

By means of the above equations y and V can be determined at any point on the (x,t)-plane by changing the grid size or shape by varying Δt and Δx.

4.3 Specified Intervals Scheme

One way to describe the specified intervals scheme for integrating the equations of gradually varied flow is to consider the (x, t)- plane subdivided into grids of equal sized rectangles, each Δx long and Δt high. The initial conditions V and y are known along the lower boundary corresponding to $t = 0$ and the upstream conditions are known along the left boundary of Figure 4.3.

Assuming that y and V are known at every grid point along the line $t = t_1 - \Delta t$ as shown in Figure 4.3, then y and V can be determined at the grid points along $t = t_1$ in the following manner. Consider that y and V are to be determined at point P. By determining the slopes of the characteristics that pass through point P, the positions where the characteristics cross the line $t_1 - \Delta t$ (points R and S) can be found. The values of depths and velocities at these points can then be calculated by interpolation equations using the grid points in the

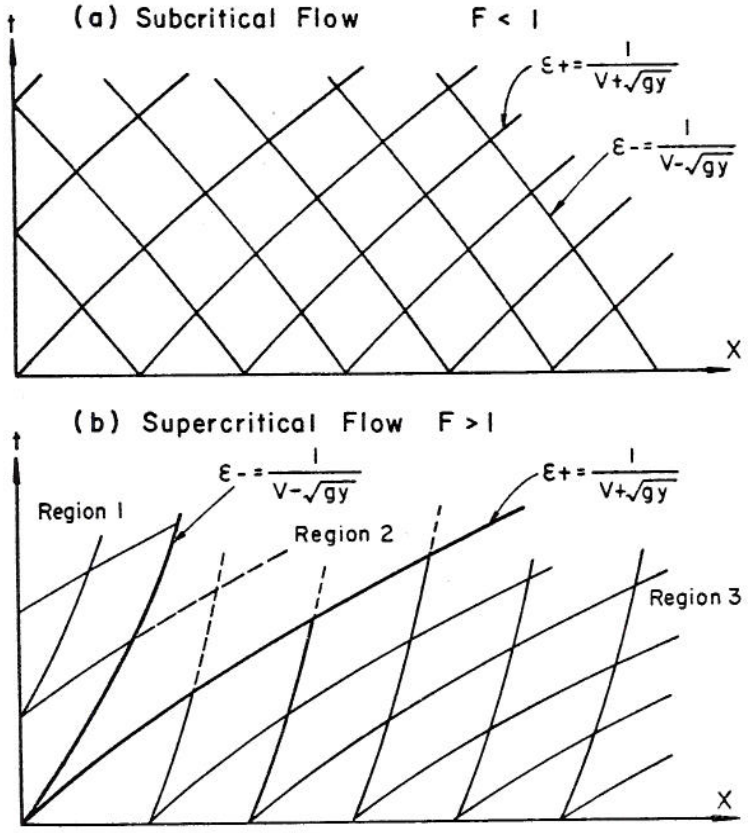

Figure 4.1 Families of Characteristic Curves for both Subcritical and Supercritical Flows

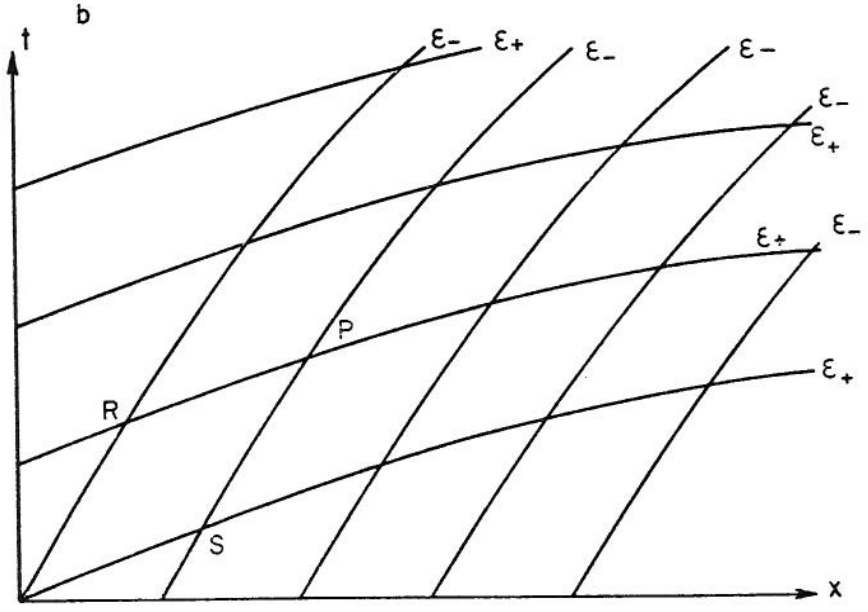

Figure 4.2 Grid for the Solution by Characteristic Grid Scheme

neighbourhood of points R and S. From these values the frictional slopes and the coefficients in Equations 3.22 and 3.23 can be evaluated, and the equations can be integrated along the characteristics to determine y and V at point P.

Equations 3.22 and 3.23 may be expressed in the following algebraic form proceeding from points R and S on the $t_1 - \Delta t$ line to the point P on the t_1 line, as

$$(F_+)_R(y_P-y_R) + (G_+)_R(V_P-V_R) + (S_+)_R(x_P-x_R) = 0 \ , \tag{4.5}$$

along the positive characteristic, and as

$$(F_-)_S(y_P-y_S) + (G_-)_S(V_P-V_S) + (S_-)_S(x_P-x_S) = 0 \ , \tag{4.6}$$

along the negative characteristic. In these equations the coefficients have

$$(F_+)_R = \left\{\left[\frac{A}{VB} - \frac{V}{g}\right]\epsilon_+ + \frac{1}{g}\right\}_R \ ,$$

$$(F_-)_S = \left\{\left[\frac{A}{VB} - \frac{V}{g}\right]\epsilon_- + \frac{1}{g}\right\}_S \ ,$$

$$(G_+)_R = \left(\frac{A}{VBg}\right)_R \ ,$$

$$(G_-)_S = \left(\frac{A}{VBg}\right)_S \ ,$$

$$(S_+)_R = \frac{A}{VB}(S_o - S_f)_R \ ,$$

and

$$(S_-)_S = \frac{A}{VB}(S_o - S_f)_S \ .$$

Using the values of V and y at points R and S, Equations 4.5 and 4.6 are solved simultaneously to determine the depth and velocity at the point P, *i.e.*,

$$D_P = \frac{\begin{bmatrix}(T_+)_R & (G_+)_R\\ (T_-)_S & (G_-)_S\end{bmatrix}}{\begin{bmatrix}(F_+)_R & (G_+)_R\\ (F_-)_S & (G_-)_S\end{bmatrix}} \tag{4.7}$$

and

$$V_P = \frac{\begin{bmatrix}(F_+)_R & (T_+)_R\\ (F_-)_S & (T_-)_S\end{bmatrix}}{\begin{bmatrix}(F_+)_R & (G_+)_R\\ (F_-)_S & (G_-)_S\end{bmatrix}} \ , \tag{4.8}$$

in which

$$(T_+)_R = (F_+)_R - y_R + (G_+)_R V_R - (S_+)_R(x_P-x_R) \ ,$$

and $(T_-)_S = (F_-)_S y_S + (G_-)_S V_S - (S_-)_S(x_P-x_S)$.

The solution is continued in the x direction first and then continued for successive values of t, at Δt intervals apart, until the flow in the channel is simulated for a specified duration.

4.4 Comparisons of Solutions Obtained by the Characteristic Grid and Specified Intervals Schemes

Some of the disadvantages in using the characteristic grid scheme are as follows.

1. The depths and velocities are obtained on the (x,t)-plane in an uneven distribution of grid points. To obtain results in an orderly distribution, interpolations for calculated depths and velocities must be carried out in the x and t directions. Any order of interpolation possesses certain numerical errors that undermine some of the precision of the characterisitc grid scheme.

2. It is difficult to space the characteristics of the same sign a suitable distance apart along the x and t axes. For example, the flow regimes in regions 1 and 3 in Figure 4.1 are independent of each other, and the flows in region 2 are dependent on conditions in region 1 and 3; therefore, it is impossible to know the spatial intervals of the characteristics in region 2 beforehand.

3. Members of the same family of characteristics in the supercritical regime may converge with flows of high Froude number. When this occurs, the depth and velocity at the grid point are no longer single-valued, and the method breaks down.

In contrast to the problem associated with the characteristic grid scheme, the specified intervals scheme has certain advantages. One of them is that the grid spacing is known beforehand. The numerical solution is also more systematic, and the depths and velocities can be obtained at grid points where adjacent characteristics converge, which is precluded in the characteristic grid scheme.

Some of the work by Zovne can be used to infer other advantages in using the specified intervals scheme. He considered hypothetical, supercritical flow in which a linearly decreasing hydrograph was simulated by both the characteristic grid and the specified intervals schemes. His results are shown in Figure 4.4. It can be seen that the solutions from the two schemes are almost identical which, in view of the difficulties of the characteristic grid scheme described above, lends support to the use of specified intervals scheme for simulating supercritical flows in this and similar studies.

Some of the assumptions necessary for using the specified intervals scheme are as follows.

1. Interpolation must be used to determine the depths and velocities at the points where the characteristics that pass through point P cross the line $t_1 - \Delta t$, (points R and S).

2. It is assumed that the slopes of the characteristics at point P are the same as at point C . In other words, it is assumed the change in slopes of the characteristics over a Δt time interval is small; if this assumption can not be made, an iterative scheme must be used to re-evaluate the slopes of the characteristic equations and in turn the values of the coefficients in Equations 4.5 and 4.6.

3. It is assumed that the curvature of the characteristics over Δt interval is negligible. Although the errors associated with the assumptions in [1] and [2] can be reduced by the refinement of the algorithm, there is no way, as yet, to reduce this error as an operating program.

4. The grid size of the specified intervals scheme must be smaller than with the characteristic grid scheme for the same degree of accuracy, since both the positive and negative characteristics that pass through point P must cross within a grid spacing in order for the interpolation equations to be valid. This condition of both positive and negative characteristics passing through a single grid spacing is sometimes referred to as the Courant condition for numerical stability, which states that $\Delta t = \Delta x/(V + \sqrt{gy})$. Although this numerical stability criterion was first used by Massau with his work on the graphical solution of the differential equations of unsteady flow, it has been referred to as the Courant stability criterion by recent researchers such as Liggett and Woolhiser (1967), Streeter and Wylie (1967), and Zovne (1970). To avoid confusion in the literature, the writers will also refer to this stability criterion as the Courant condition.

The specified intervals scheme is used to determine the criterion for amplification in this study. Some of the limitations with regard to accuracy of the scheme as described in the four assumptions discussed above will be discussed in more detail in the next section.

4.5 Accuracy of Specified Intervals Scheme in Simulating Supercritical Flows

4.5.1 Introduction. It has been demonstrated by Pinkayan and Barnes (1967) that the smaller the Δx size in the specified intervals scheme, and thus the smaller the Δt used in order to satisfy the Courant condition, the more accurately the scheme will compare with observed flows in the subcritical regime. In the supercritical regime, however, there are few observed flows with which comparisons can be made.

Zovne, in his comparisons of characteristics grid and specified intervals schemes, assumed that the slopes of the characteristics changed a negligible amount over the Δt interval at any grid point along the channel. He used two point interpolations to determine the positions (points R and S) in Figure 4.3 where the characteristics cross the line $t_1 - \Delta t$ from the values of the dependent variables at the grid points and he evaluated the values of the coefficients of Equations 4.5 and 4.6 at points R and S, respectively. The comparison of results obtained from the specified intervals scheme with the results obtained from the characteristic grid scheme shows good correlation as shown in Figure 4.4. Zovne also stated that the use of a second order interpolation equations and the averages of the values of frictional slopes between points P and R and between points P and S improved the accuracy of the scheme, although their use was not warranted in his study.

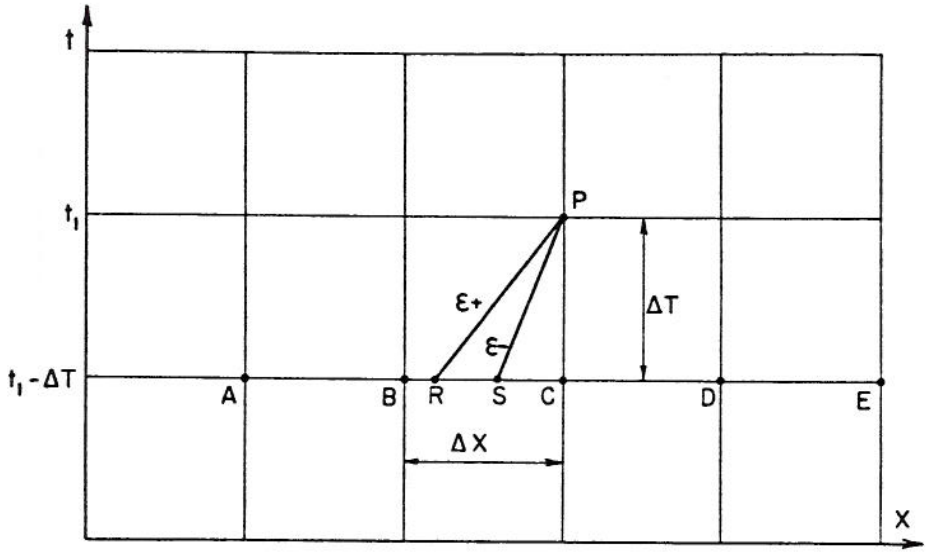

Figure 4.3 Grid for the Solution by Specified Intervals Scheme

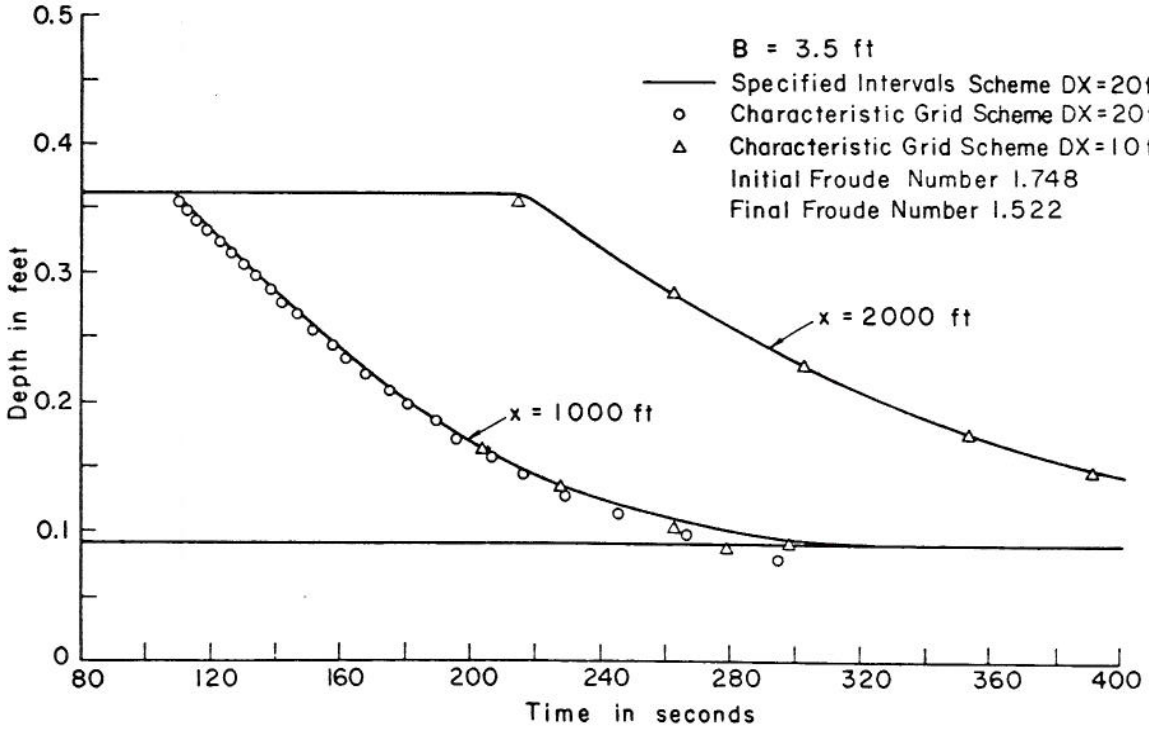

Figure 4.4 Comparison of Solution by Characteristic Grid and Specified Intervals Schemes

A term-integration technique – that has not appeared as yet in the literature pertaining to the specified intervals scheme – will be used throughout the remainder of the text. This technique is as follows. Interpolation equations of various order are used to determine values of the dependent variables at points R and S after the positions on the $t_1 - \Delta t$ line of the latter are found from the slopes of the characteristics. Then the coefficients of Equations 4.5 and 4.6 are evaluated at either point C or at points R and S. Once the equations have been integrated, the slopes of characteristics of point P may or may not be redetermined and the above procedure is repeated until two successive values of characteristic slopes are within a specified tolerance. The technique from determining where the characteristics cross the t_1-Δt line to finding the values of the dependent variable, with or without iterations, at point P will be called an integration technique. Moreover, an integration technique that includes a particular order of interpolation equations to determine the values of the dependent variables at points R and S is prefixed with the order of the interpolations. Therefore, a technique that uses third order interpolation equations is called a third order integration technique.

In this study, where the flow conditions at which a wave neither amplifies nor attenuates are to be determined, the most accurate technique possible must be used. The tests conducted to determine the refinements to the basic first order integration technique to obtain the most accurate algorithm were simulated in a rectangular shaped channel, the sides of which are hydraulically smooth. A constant base flow governed by the Chézy resistance relation is introduced into this channel. The inlet conditions are sinusoidal hydrographs superimposed on the base flow. The depth-discharge relation at the inlet (rating curve) is the normal depth relation.

The refinements that are made to the specified intervals scheme to improve its accuracy are: (a) decreasing the grid size; (b) increasing the order of the interpolation equations used to determine the values of the dependent variables at points R and S ; (c) evaluating the coefficients of Equations 4.5 and 4.6 at points R and S instead of at point C , where most of the current investigators have evaluated them – Henderson (1966), Streeter and Wylie (1967), and Yevjevich and Barnes (1970); (d) once the depth and velocity have been calculated at point P using the characteristic slopes at point C ; then the characteristic slopes are re-evaluated at point P , and new depth and velocity determined at point P . This is continued by using an iterative procedure until successive values of calculated characteristic slopes are within a particular tolerance. The tolerance used for this study was 0.00001 feet.

The last refinements, (b), (c), and (d) are discussed under the subject of integration techniques. The effects of the first refinement is as follows.

4.5.2 Grid size. Once the Δx size has been chosen then the Δt size is specified by the Courant stability condition. Therefore, by varying the Δx the size of the grid mesh is also varied. Considering a wave flowing on a base flow of high Froude number such that the wave should amplify throughout the length of the channel, then the grid size should be small enough so that the simulated wave does amplify throughout the length of the channel.

Figure 4.5 shows the results of a wave resulting from a sinusoidal inflow hydrograph of 20 seconds duration with a discharge ratio, $Q_p/Q_b = 1.05$ flowing in a rectangular channel 1.2 feet wide on a base flow with a depth of 0.25 feet and a Froude number of 3.0. This figure shows the dimensionless peak wave depth at 40 feet from the inlet versus the Δx used in the integration.

The specifications of the integration technique are such that the slopes of the characteristics at point P are the same as at point C ; first order interpolations are used to determine the values of dependent variables at points R and S , and the coefficients of Equations 4.5 and 4.6 were evaluated at points C .

It may be seen that when Δx is larger than two, the wave peak depth at 40 feet from the inlet is less than the peak depth at the inlet. When the Δx is less than two feet, the peak wave depth at 40 feet are larger than at the inlet. Since the discharge ratio is small and the base flow width-depth ratio is large, $B/Y_b = 4.8$, then by the theory of small disturbance on uniform flow, the peak depth should increase as the wave travels along the channel (Koloseus and Davidian). Therefore, for the inflow conditions tested a Δx smaller than two feet should be used. It may be seen also from Figure 4.5 that when Δx is decreased from two feet to one foot, there is a very small increase in wave depth at 40 feet. This may be better seen in Figure 4.6 where the peak

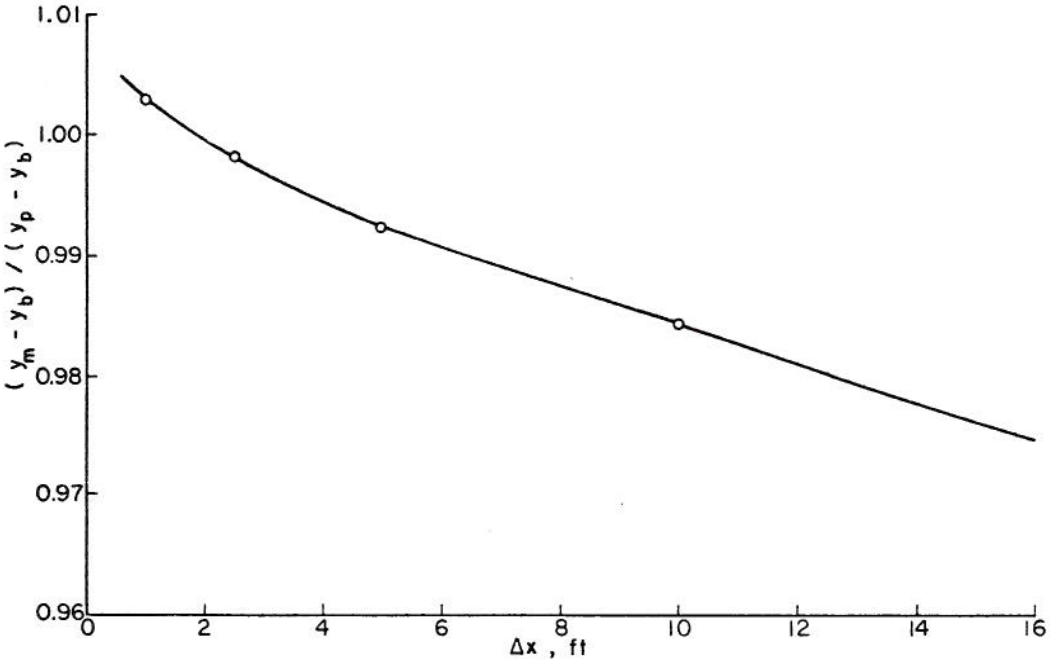

Figure 4.5 Effect of Grid Size on Peak Depths
F_b = 3.0, Q_p/Q_b = 1.05, υ_b = 1.06
υ_p = 1.04
lst Order Interpolations x = 40 ft

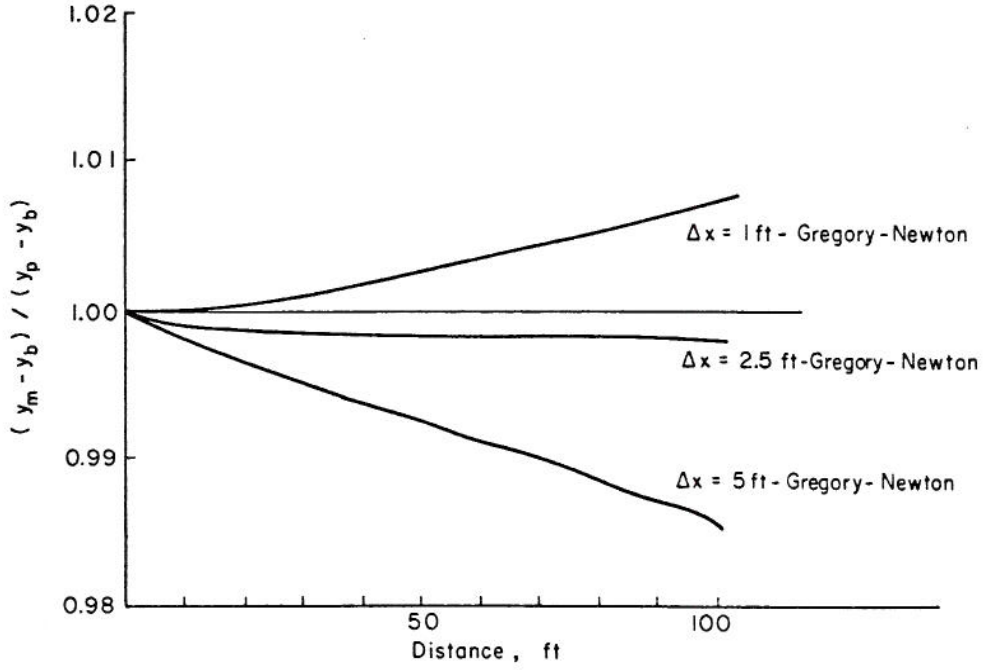

Figure 4.6 Effect of Grid Size on Peak Depths
F_b = 3.0, Q_p/Q_b = 1.05, υ_b = 1.06
υ_p = 1.04

wave depth is plotted against distance along the channel. It is concluded that the smaller the Δx size used in the simulations, the better the accuracy of the simulation, although there is a Δx size below which very little improvement in accuracy is obtained. It would be also noted that improved accuracy must be weighed against increased computer time and the computer memory storage required to obtain it.

4.5.3. Integration techniques. To find the depths and velocities of points R and S from the known values of depths and velocities at the grid points in the neighborhood of points R and S intepolation equations must be used. Two types of interpolation equations were used and compared in this study to determine the better one to use in the integrations. The first interpolation equation, generally known as the Gregory-Newton equation, makes use of various order of finite difference approximations to derivatives. The second type, the Lagrangian interpolation equation, makes use of functional values at the grid points together with corresponding values of the independent variable. The second order equation for both types for y_R are given below.

The Gregory-Newton interpolation equation for the depth at point R is

$$y_R = y_B + \frac{C_R}{\Delta x}(y_C - y_B) + \frac{C_R^2}{2\Delta x^2}(y_D - 2y_C + y_B) \tag{4.9}$$

in which $C_R = x_R - x_B$. The Lagrangian interpolation equation for the depth at point R is

$$y_R = \frac{(U_R-1)(U_R-2)}{2} y_B - U_R(U_R-2) y_C + \frac{U_R(U_R-1)}{2} y_D , \tag{4.10}$$

in which $U_R = (x_R - x_B)/\Delta x$.

The effects of the two interpolation equations may be seen in Figure 4.7 where the results of an attenuating wave produced by a sinusoidal inflow hydrograph of 20 seconds duration are shown. This figure shows the dimensionless peak wave depth graphs for the second order integration techniques described above. The coefficients of the ordinary differential equations, 4.5 and 4.6, are evaluated at points R and S , and no iterative procedure is used to refine the slopes of the characteristics which are evaluated at point C . The Δx size used in this simulation, as well as all subsequent simulations in the study, is five feet. The Vedernikov number of the flow is less than one everywhere on the wave profile. The dimensionless peak wave depth is also plotted in Figure 4.7 for a first order integration technique, which has the same equation for both the Gregory - Newton and Lagrangian interpolation equations. It may be seen that the second order technique gives higher peak depths than the first order technique. Also it may be noticed by comparing the results of the second order technique that the Lagrangian interpolation equation gives somewhat higher peak wave depths and a smoother curve than the Gregory - Newton equation gives.

The dimensionless peak wave depth is plotted in Figure 4.8 for the same conditions as in the Figure 4.7, except that the Froude number of the base flow has been doubled so that the Vednerikov number of the flow over the wave profile is now greater than one. It is clearly seen that the first order integration technique does not simulate an amplifying wave with the grid size used ($\Delta x = 5$ ft). The second order techniques produce wave amplification with the Lagrangian interpolation equation giving somewhat higher peak depths.

Of greater consequence is that the Gregory-Newton equation initially produces a dip in the maximum wave peak. This dip represents a condition where the peak depths decrease initially as the wave travels along the channel before the peak depths start to increase. This condition is due to the following reasons. At the first grid point from the inlet where the depths and velocities are to be determined, points B , C and D must be used in the interpolating equations as shown in Figure 4.3. At the other grid points along the line $t_1 - \Delta t$, point A is closer to points R and S than point D , so that it would be logical to use point A . Therefore, with the second order integration techniques, points B , C and D are used at the first grid point in from the upstream boundary, and points A , B , and C for the rest of the grid points along the line $t_1 - \Delta t$. From Figure 4.8 it may be learned that the shifting of the interpolating mesh has an adverse effect on the results produced by the integration technique that uses the Gregory-Newton equation.

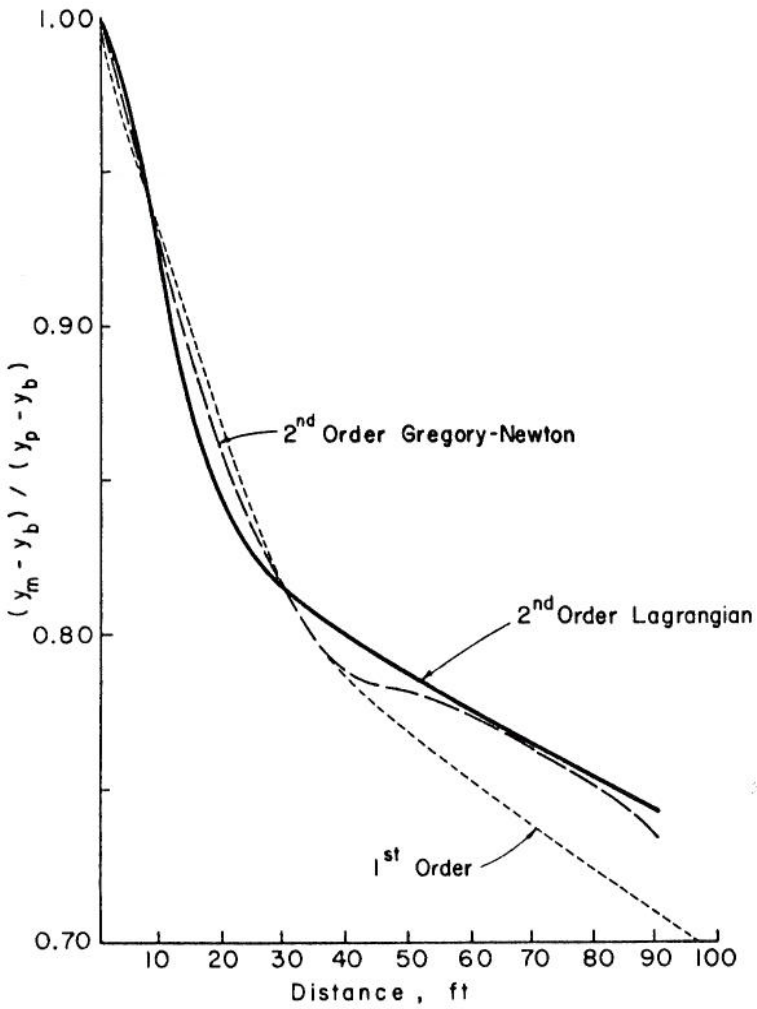

Figure 4.7 Effects of Type of Interpolation Equation on Peak Depths for an Attenuating Wave
F_b = 1.5, Q_p/Q_b = 1.05, v_b = 0.53, v_p = 0.52

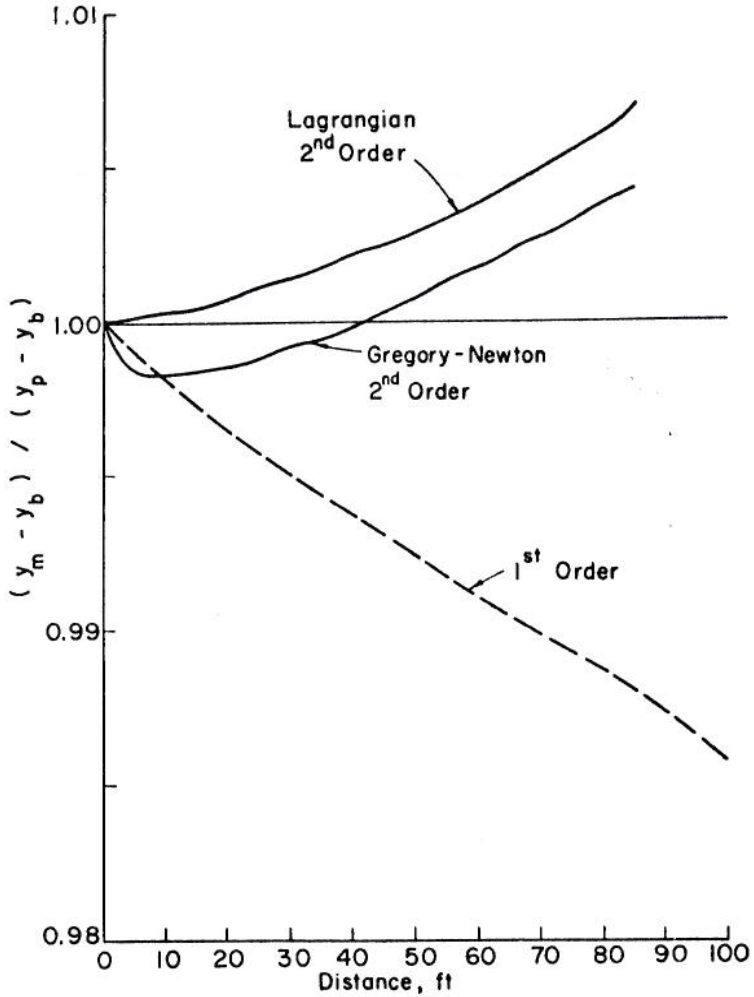

Figure 4.8 Effects of Type of Interpolation Equation on Peak Depths for an Amplifying Wave
F_b = 3.0, Q_p/Q_b = 1.05, v_b = 1.06 v_p = 1.04

Figures 4.9 through 4.14 show the effects of the third order Lagrangian integration techniques with different positions at which the coefficients of the difference equations (Equations 4.5 and 4.6) are evaluated and the iterative procedures of calculating the slopes of the characteristics for both amplifying and attenuating waves. The top portion of Figure 4.9 shows the plot of dimensionless peak wave depths against distance for an attenuating wave ($F_b = 1.5$) obtained by the third order Lagrangian integration technique with the coefficients evaluated at points R and S and the slopes of the characteristics recalculated by an iterative procedure until the two successive iterations show the same values of slopes to the tolerance of 0.00001 foot. The bottom portion of the graph shows the relative error of the peak depths for various integration techniques compared to the peak depths produced by the technique described above, which is labelled L5, *i.e.*, for the first order integration technique $(y_{L1} - y_{L5})/y_{L5}$ is plotted against distance along the channel, where L1 designates the first order integration technique with the coefficients evaluated at point C. The other integration techniques are designated as follows: L2 the second order integration technique with the coefficients evaluated at point C; L3 the third order integration technique with the coefficients evaluated at point C, and L4 the third order integration technique with the coefficients evaluated at points R and S.

With the flow conditions shown in Figure 4.9 the relative error for the first order integration technique compared with the third order technique is so large that the curve does not plot on the graph. The third order integration technique, L3, produces smaller errors than the second order; the third order technique with the coefficients evaluated at points R and S, L4, produces a relatively much smaller errors. There is a larger difference between L4 and L3 integration techniques than between L2 and L3 techniques. There is a difference also between L4 and L5; however, this difference is much smaller than between the other techniques.

Figure 4.10 shows the results of different integration techniques for the same conditions as in Figure 4.9 except the discharge ratio of the inflow hydrograph is 1.30, or six times the wave peak discharge than in the previous case. The results are relatively the same, *i.e.*, the L4 technique is closer to the L5 technique than the L3 technique is; however, the relative errors are larger by at least an order of magnitude.

Figures 4.11 and 4.12 show the relative errors of the different integration techniques for an amplifying wave with the Vedernikov number greater than one over the wave profile. In the upper part of Figure 4.11, the dimensionless wave peak depths are plotted against distance along the channel with the peak depth increasing with distance using the L5 technique. In the bottom portion of the plot the relative errors of L1 and L2, *i.e.*, first and second order integration techniques, are shown. Figure 4.12 gives the latter plot but it is enlarged to show the relative error for the L2, L3, L4, and L5 techniques. Again L3 technique produced a smaller relative error than L2 technique, and L4 technique in turn produced a smaller relative error than L3 technique. This sequence of relative errors is the same as was found for an attenuating wave. The relative errors are an order of magnitude smaller than for the attenuating wave with the same discharge ratio, *i.e.*, $Q_p/Q_b = 1.05$.

Figures 4.13 and 4.14 also show the relative errors of maximum peak depths resulting from the different integration techniques. Here the discharge ratio is the same as in Figure 4.10; however, the Froude number of the base flow is now 3.0. This base flow Froude number combined with the discharge ratio of 1.3 produces an attenuating wave depicted in the upper portion of Figure 4.13 and determined by the L5 technique. The relative errors have the same order as before; however, the errors are an order of magnitude smaller than with the smaller Froude number of the same discharge ratio.

It may be concluded that the third order Lagrangian integration technique with the coefficients evaluated at points R and S, L4, gives an accurate algorithm. The third order Lagrangian interpolation equation for y_R (referring to Fig. 4.3 for the grid points) is

$$y_R = -\frac{(U_R-1)(U_R-2)(U_R-3)}{6} y_A + \frac{U_R(U_R-2)(U_R-3)}{2} y_B - \frac{U_R(U_R-1)(U_R-3)}{2} y_C + \frac{U_R(U_R-1)(U_R-2)}{6} y_D, \quad (4.11)$$

in which $U_R = (x_R - x_A)/\Delta x$. The increase in accuracy obtained by recalculating the characteristic slopes in the integration technique, L5, is small

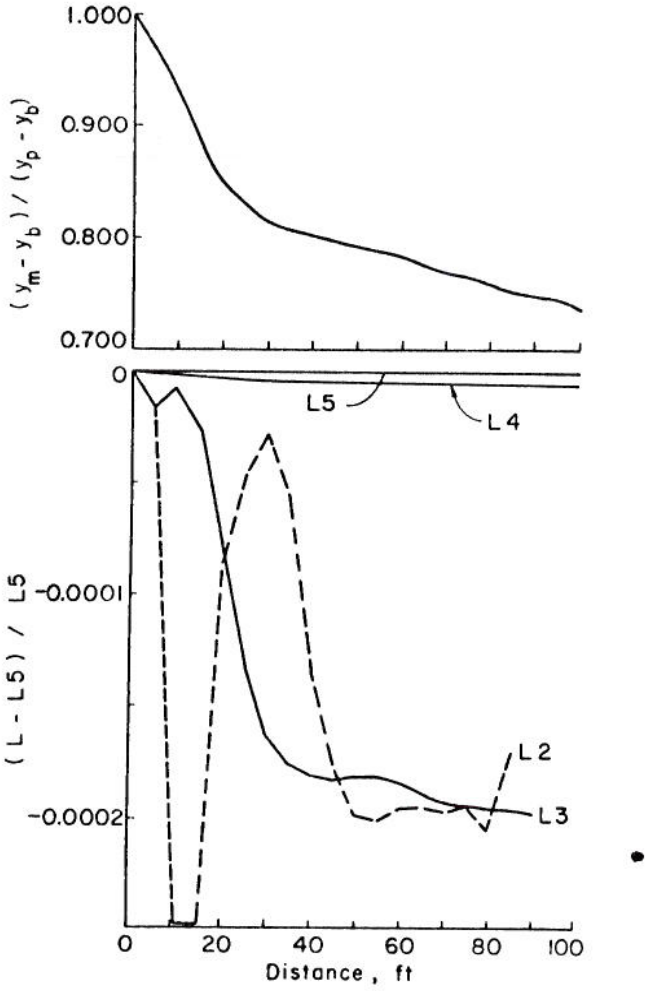

Figure 4.9 Effects of Integration Technique on Peak Depths for an Attenuating Wave $F_b = 1.5$, $Q_p/Q_b = 1.05$, $v_b = 0.53$, $v_p = 0.52$

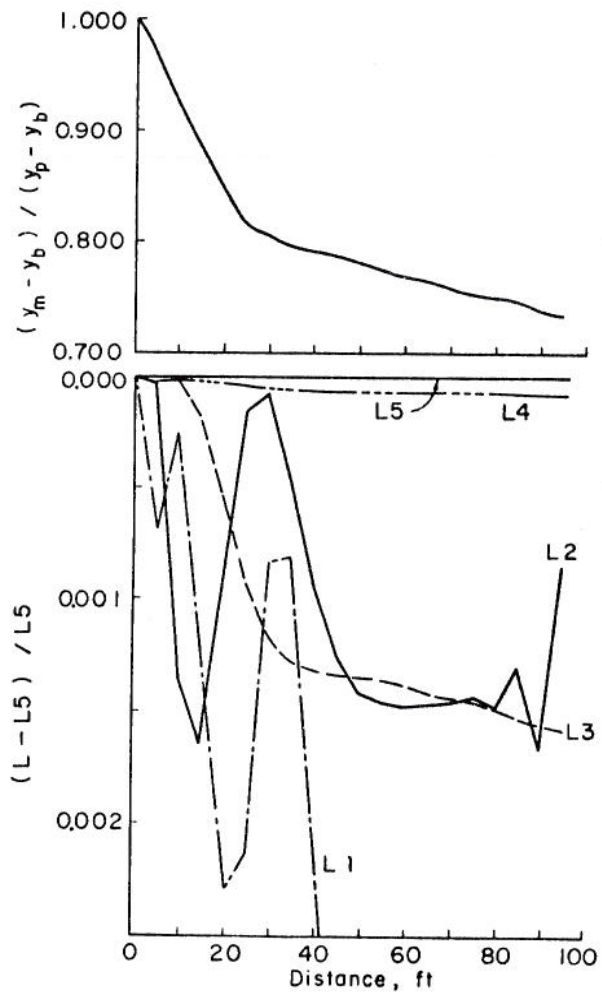

Figure 4.10 Effects of Integration Technique on Peak Depths for an Attenuating Wave $F_b = 1.5$, $Q_p/Q_b = 1.30$, $v_b = 0.53$, $v_p = 0.48$

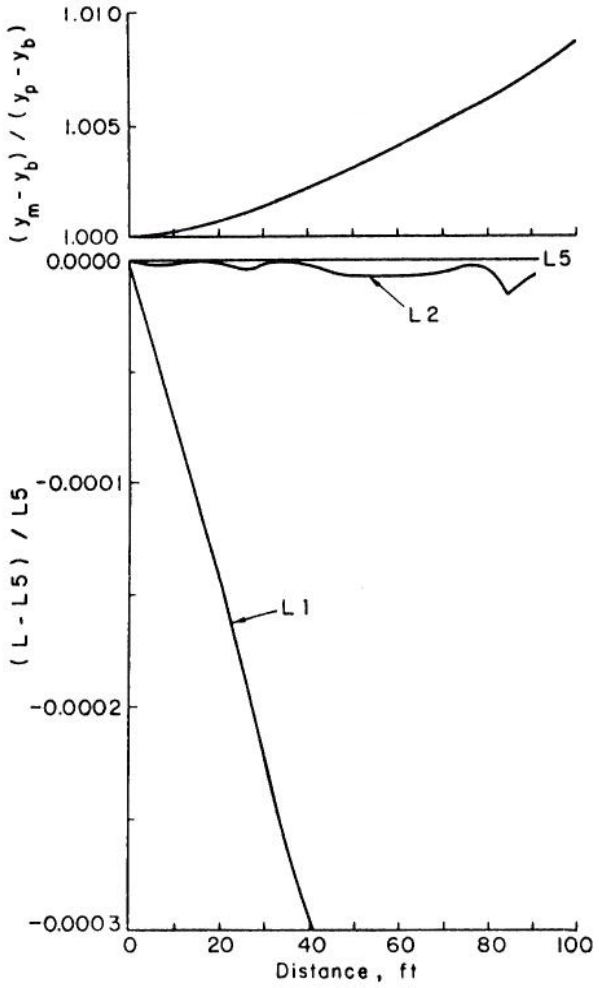

Figure 4.11 Effects of Integration Technique on Peak Depths for an Amplifying Wave $F_b = 3.0$, $Q_p/Q_b = 1.05$, $\upsilon_b = 1.06$, $\upsilon_p = 1.04$

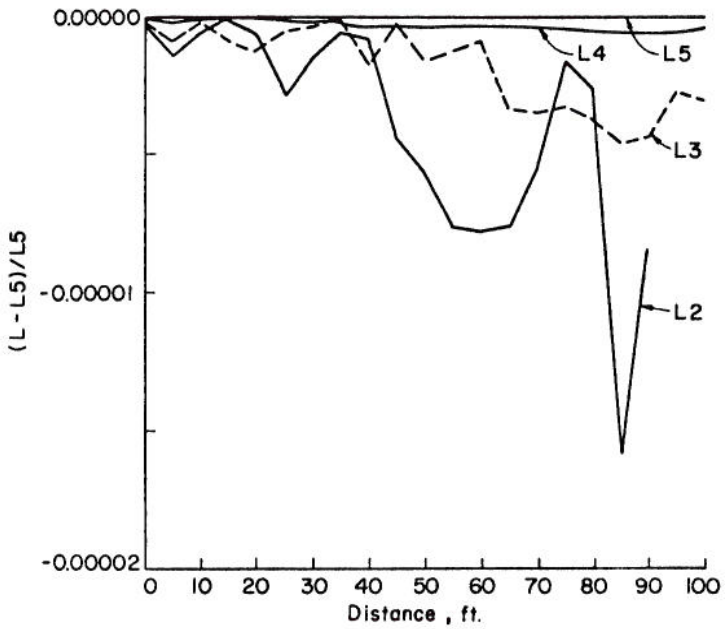

Figure 4.12 Effects of Integration Technique on Peak Depths for an Amplifying Wave $F_b = 3.0$, $Q_p/Q_b = 1.05$, $\upsilon_b = 1.06$, $\upsilon_p = 1.04$

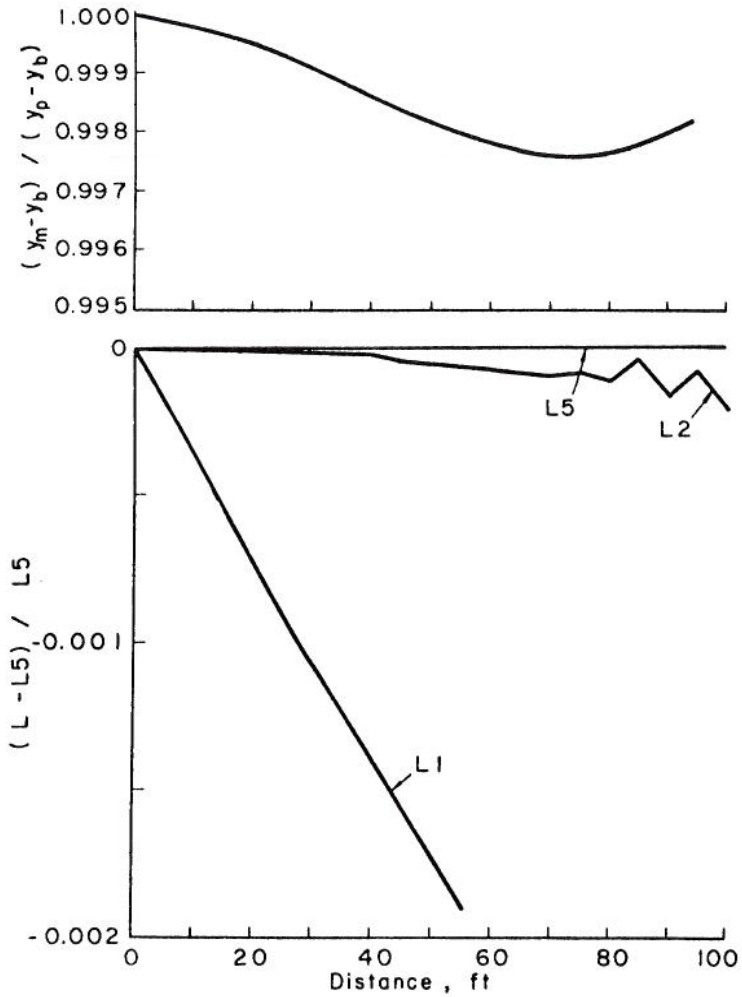

Figure 4.13 Effects of Integration Technique on Peak Depths for an Attenuating Wave $F_b = 3.0$, $Q_p/Q_b = 1.30$, $\upsilon_b = 1.06$, $\upsilon_p = 0.96$

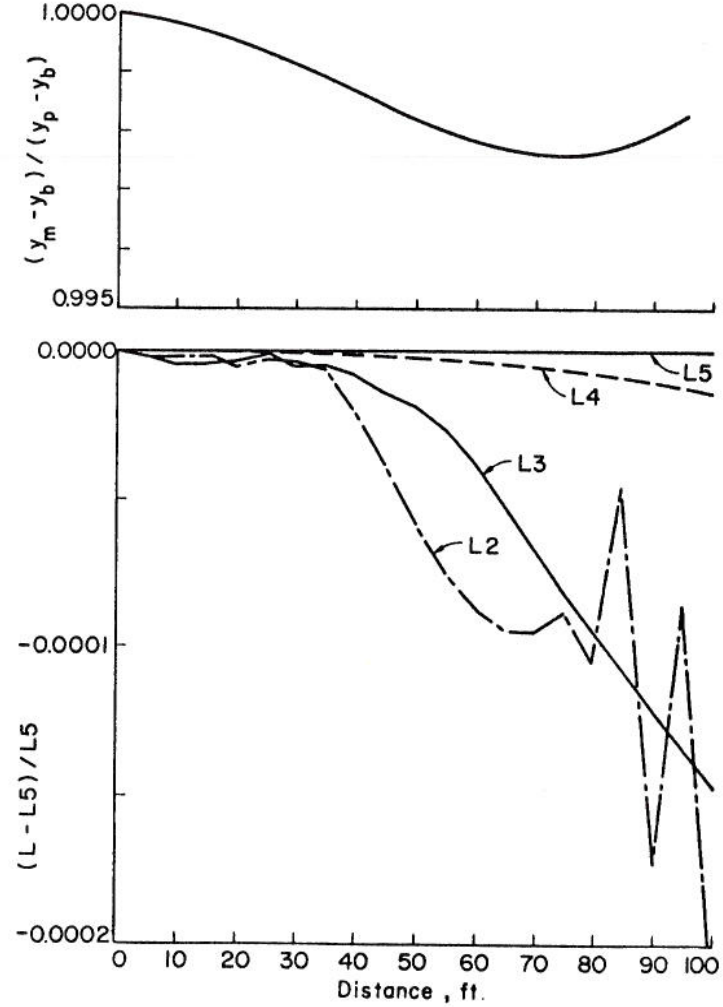

Figure 4.14 Effects of Integration Technique on Peak Depths for an Attenuating Wave $F_b = 3.0$, $Q_p/Q_b = 1.30$, $\upsilon_b = 1.06$, $\upsilon_p = 0.96$

compared to the L4 technique, and the use of this technique is not warranted in view of the increased computer time required. It may be also concluded that the relative errors increase with discharge ratio and distance along the channel; however, they decrease with higher base flow Froude number. These properties are considered in the design of experiments that are used to study the criterion of wave amplification.

4.5.4 Flow acceleration considerations. Both Chow (1959) and Henderson (1966) state that waves are gradually varied when the vertical accelerations are small compared to the horizontal accelerations. Rapidly varied flow occurs when this is not true. Because of this it was considered necessary to ensure that the vertical accelerations would be small for the flow conditions simulated so that the equations would represent the physical flow correctly. An extensive review of the literature, however, reveals that no author has defined what magnitude "small" is in this context, except by stating that with a small acceleration ratio the pressure distribution of the flow would be hydrostatic. To ensure that the waves studied can be adequately described by the equations of gradually varied flow, an algorithm using finite difference approximations to derivatives is used to determine the accelerations in the normal and parallel directions to the channel bed of the wave surface at a given distance along the channel from the inlet. Since in this study $\alpha = \beta = 1$, the flow is assumed to have a uniform velocity distribution; therefore, the relative movements of the wave surface represents the movements of water particles in the wave.

Figures 4.15 and 4.16 represent the cases of attenuating waves. It may be seen from Figure 4.15 that the accelerations parallel to the bed are much larger than the accelerations normal to the bed over the wave crest except at the peak. The accelerations ratios are shown at the top of Figure 4.16 and they are always smaller in magnitude than 0.25 except at the peak where there is a large ratio. Referring to Figure 4.15 it may be seen that this large ratio occurs only when the accelerations parallel to the bed are very small, not when the normal accelerations are large. The amplifiying wave conditions are shown in Figure 4.17 and 4.18. In these figures it may be seen that again the normal accelerations are small when compared with accelerations parallel to the bed. The magnitudes of the normal accelerations for an amplifying wave are much smaller than in the attenuating wave, by an order of magnitude. The normal accelerations are smaller than 0.002 ft/sec^2 which is extremely small compared to the acceleration due to gravity.

The acceleration ratios may reach values that are greater than one in both attenuating and amplifying waves, which by itself may preclude the use of the partial differential equations of gradually varied, free surface flow to correctly simulate the flow conditions. In these cases of amplifying and attenuating waves, the maximum values of the acceleration ratio occur when the accelerations parallel to the bed have the smallest values on the wave profile, *i.e.*, where the flow velocities are at a maximum and not at the points where the normal accelerations are at a maximum. In view of the magnitude of these accelerations, and their relatively constant value over a wave crest region, it may be assumed that the differential equations of gradually varied flow are valid for the range of conditions being studied.

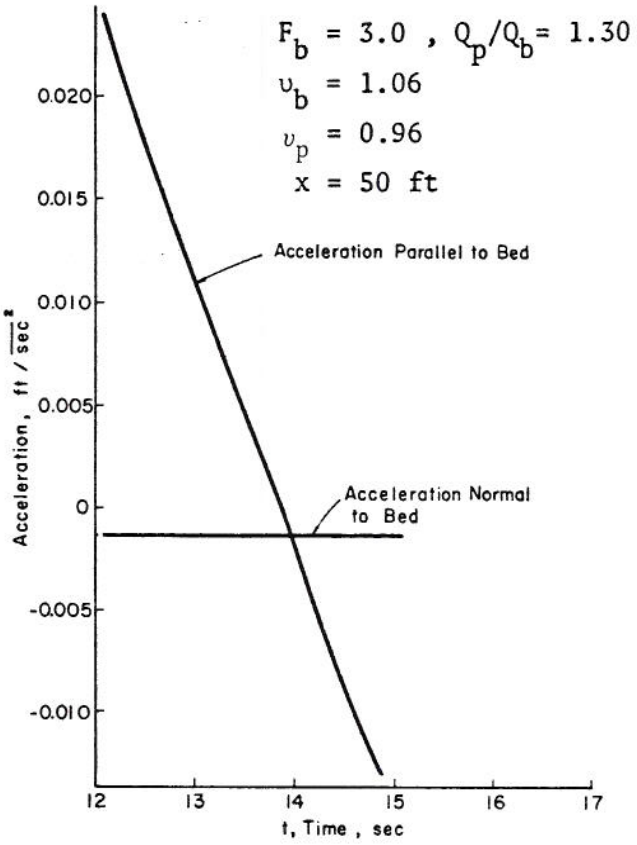

Figure 4.15 Acceleration on the Crest of an Attenuating Wave

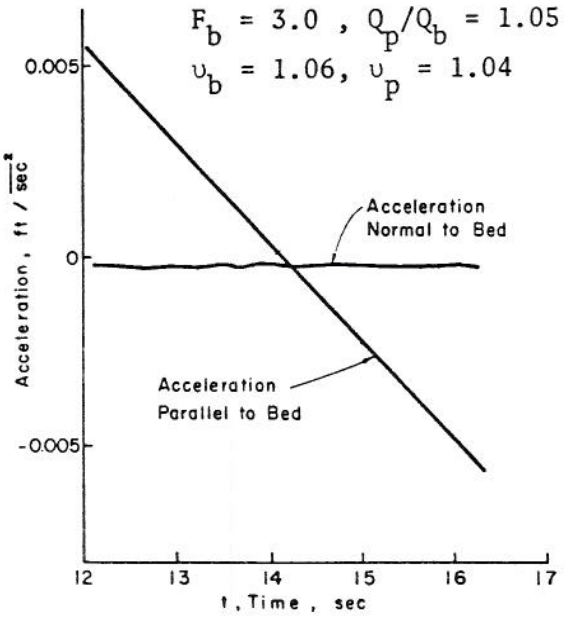

Figure 4.17 Accelerations on the Crest of an Amplifying Wave

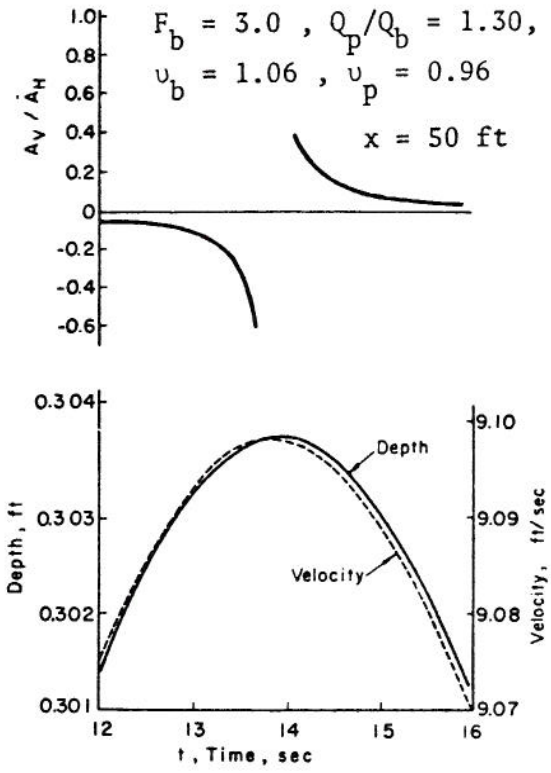

Figure 4.16 Acceleration Ratios, Depths and Velocities on the Crest of an Attenuating Wave

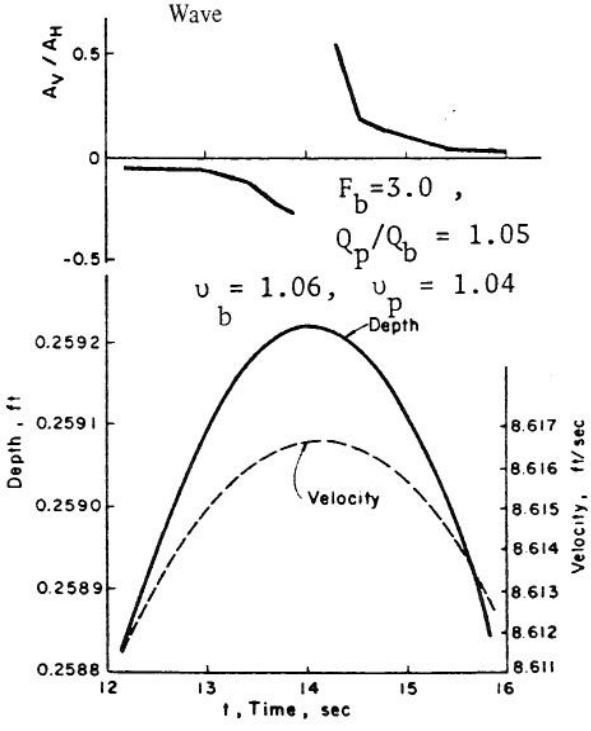

Figure 4.18 Acceleration Ratios, Depths and Velocities on the Crest of an Amplifying Wave

Chapter 5

AMPLIFICATION CRITERION

5.1 Introduction

The objective of the study is stated in Chapter 1. Some of the previous work on uniform flow and examples of the problems in the physical domain are covered in Chapter 2. The methods of mathematical integration of the equations of gradually varied flow are discussed in Chapter 3. The two numerical schemes of the method of characteristics are treated in Chapter 4, and the superiority of the specified intervals scheme over the characteristic grid scheme is shown. The specified intervals scheme is then used to simulate flows in a channel with supercritical slopes to determine the amplification criterion of gradually varied, single peaked waves. Before discussing the simulations and results, however, the specifications of the channel and flow regime are described.

5.2 Boundary Conditions

5.2.1 Initial conditions. All numerical experiments are conducted with velocities in the supercritical regime. The base flow depth was specified beforehand, and it depends upon the width-depth ratio required. The slope of the channel was determined to give a particular Froude number for the base flow. Therefore, the initial conditions are that the depth and velocity are constant along the channel with a particular Froude number at the grid points, spaced five feet apart, along the x axis of the (x - t)-plane.

5.2.2 Inlet conditions. On the above base flow both sinusoidal and asymmetric inflow discharge hydrographs are introduced. The three inflow hydrographs shapes used are shown in Figure 5.1. The equation of the inflow discharge function is:

$$Q(t) = Q_b + \frac{(Q_p - Q_b)}{\lambda} e^{\theta t} \sin t \qquad (5.1)$$

in which $\lambda = e^{\theta \tan^{-1}(-1/\theta)} \sin(\tan^{-1}(-1/\theta))$, with λ the maximum value of $e^{\theta t} \sin t$ term, and the use of which ensures that the maximum values of Q(t) is Q_p.

When $\theta = 0$, the hydrograph is symmetrical and is sinusoidal. When $\theta < 0$, the hydrograph is asymmetric with an advanced peak; and when $\theta > 0$, the hydrograph is asymmetric with a retarded peak. The depth at a given time, t, is determined by the normal depth relation for a particular discharge. The velocity is then determined by using the continuity equation.

There may be some question whether the normal depth relation correctly simulates the flow conditions at the inlet. It could be envisaged that with some inlet conditions the flow would enter the channel with both vertical and horizontal components of acceleration, which the normal depth relation does not represent. Also, there may be many relations between depth and velocity at the inlet for steady flow. One extreme would be to consider a head gate in which the inlet depth remained constant and the velocity varied with the head on the gate. The other extreme would be when the velocity remained relatively constant and the depth changed. For this study it is assumed that a normal depth relation is applicable in order to determine the amplification criterion. This investigation shows that the results found for this relation are adaptable for other steady state relations and for the unsteady conditions at the inlet provided the relation between depth and velocity is known.

Figure 5.2 shows a dimensionless peak wave depth against distance plot for a sinusoidal inflow hydrograph. This figure shows the conditions where the maximum depth decreases initially on entering the channel, then after a particular distance along the channel, the peak depths begins to increase. At 100 feet from the inlet the peak depth is still increasing. By taking the depth and velocity hydrographs at this

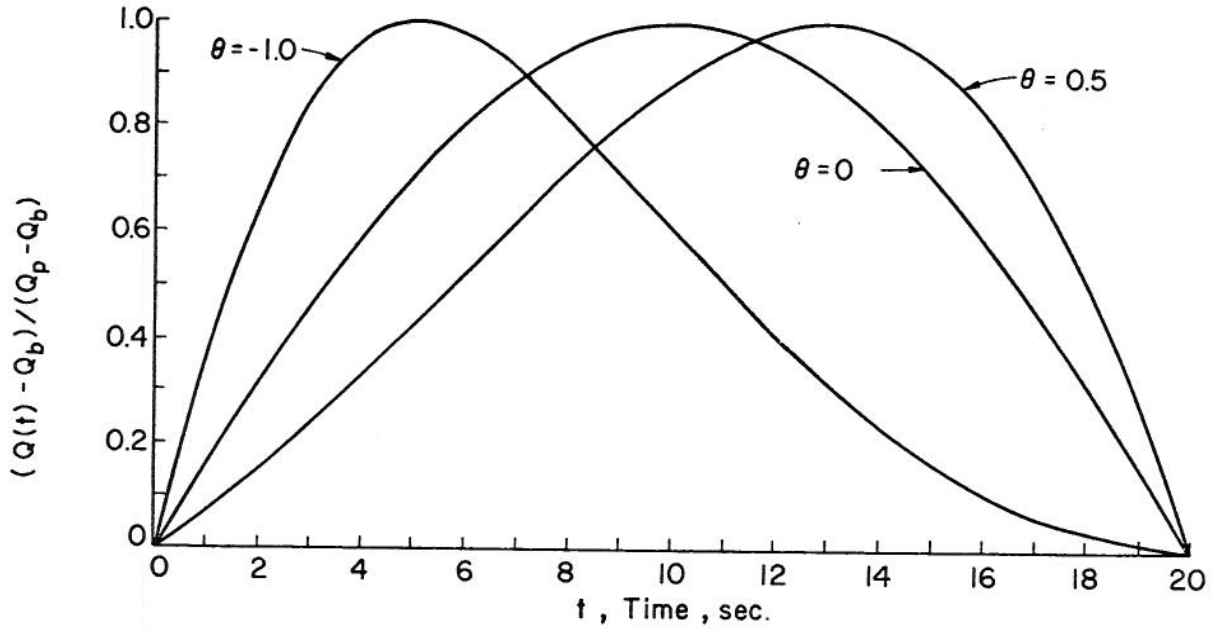

Figure 5.1 Inflow Hydrograph Shapes

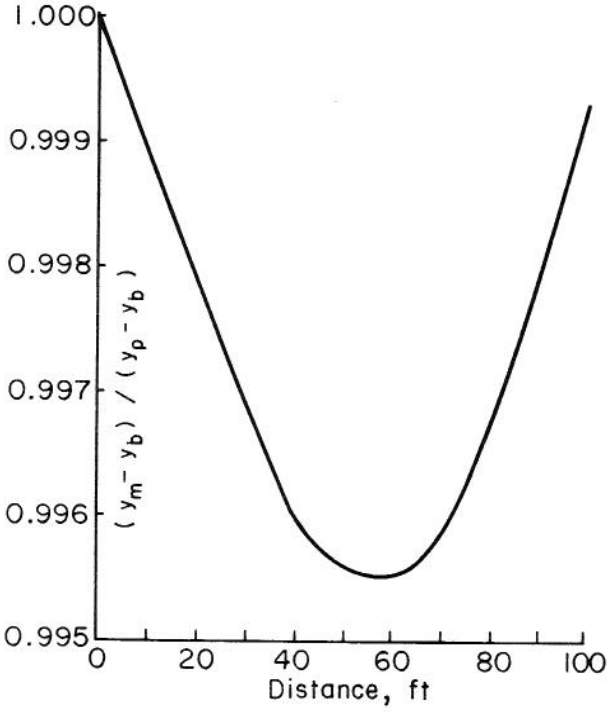

Figure 5.2 Dimensionless Peak Wave Depth versus Distance for an Amplifying Wave using Normal Depth Relation at Inlet F_b = 3.0, Q_p/Q_b = 1.2, v_b = 1.06, v_p = 0.99
1st Order Interpolations

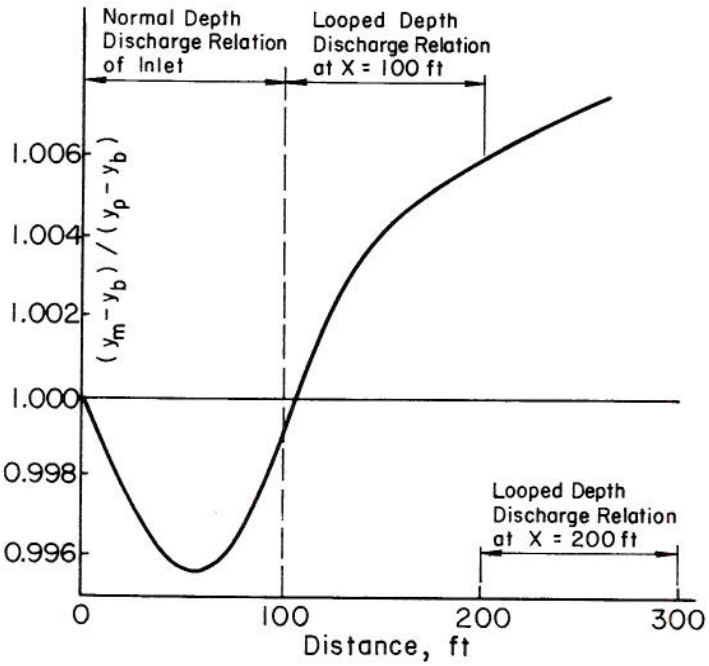

Figure 5.3 Dimensionless Peak Wave Depth versus Distance for an Amplifying Wave F_b = 3.0, Q_p/Q_b = 1.2, v_b = 1.06, v_p = 0.99
1st Order Interpolations

distance (the depth-discharge relation is now looped) and using them with an iterative approach as the inlet conditions for another channel of the same dimensions and base flow discharge, another dimensionless peak wave depth plot is obtained. This is shown in Figure 5.3. The procedure is then repeated for another 100 feet of channel, and still yet another dimensionless peak wave depth plot is obtained. The results of this procedure are also shown in Figure 5.3. Although a dip in peak wave depth plot occurs because of the normal depth relation at the inlet, the two maximum peak depth plots resulting from the looped inlet conditions for the two subsequent channel lengths do not have dips: the peak depths increase along the whole lengths of the channels. If one imagines a channel 300 feet long consisting of three equal lengths, the inlet conditions of the first governed by the normal depth relation, and the beginnings of the other lengths governed by the looped depth-discharge relations, then the maximum peak depth plot for 300 feet can be drawn. The resulting curve as shown in Figure 5.3 is smooth. The peak depths at the upstream end of the 100 to 200 foot length and the 200 to 300 foot lengths – at the 100 and 200 foot stations, respectively – have the same values of depths and velocities as at the downstream end of the length of channel immediately upstream, *i.e.*, the 0 to 100 foot and 100 to 200 foot lengths.

It may be concluded, therefore, that the normal depth inlet relations do not correctly simulate the gradually varied flow. This is to be expected since the inlet conditions are time varied and the wave possesses accelerations at the inlet that are not taken into account. This limitation of the inlet conditions will affect the amount of amplification or attenuation of a wave; however, it does not influence the flow conditions that govern whether a given wave will amplify or attenuate.

5.3 Flow Simulations

5.3.1 Choice of width-depth ratio. Figure 5.4 relates the discharge ratio at which the Vedernikov number, υ_p, of the peak is equal to one against the width-depth ratio, B/y_b, for a flow depth of 0.25 ft. It is shown later that this number is the criterion for amplification. With the small width-depth ratios the discharge ratio for $\upsilon_p = 1$ is also very small, *i.e.*, about 1.0, thereby making it difficult to determine whether a wave is attenuating or amplifying in view of the precision of the numerical algorithm. With large width-depth ratios, the discharge ratio at which $\upsilon_p = 1$ is very large. The slopes of the characteristics for the flow on the wave crest under these conditions are mild which results in small time intervals in the grid mesh of the specified intervals scheme and long durations of computer time required for the integrations.

The previous chapter has shown that the larger the discharge ratio the less accurate is the integration technique. Therefore, an intermediate width-depth ratio was used in order to satisfy these limitations. A base flow width-depth ratio of 4.8 is chosen, which is obtained with a channel width of 1.2 feet and a depth of 0.25 foot.

5.3.2 Amplification criterion. Figure 5.5 shows the peak wave depth, in dimensionless form, plotted against distance for various discharge ratios, Q_p/Q_b which result from a sinusoidal inflow hydrograph of 20 seconds duration superposed on the base flow. The Chézy resistance law was used throughout this study, *i.e.*, $b = 0$ in $f = a(R_e)^b$. The base flow Froude number is 3.0 with a width-depth ratio of 4.8. The curves in Figure 5.5 represent different discharge ratios. The Vedernikov number of wave peak, υ_p, at the inlet is labelled alongside each curve. It may be seen that when υ_p is greater than one, the wave amplifies along the channel. When the υ_p is less than one, the wave attenuates along the channel except for the wave whose υ_p is equal to 0.994 ($Q_p/Q_b = 1.2$). This wave initially attenuates and then starts to amplify. It may be also asked whether the wave with $Q_p/Q_b = 1.3$ would not start to amplify in a longer channel. The peak wave plot for Q_p/Q_b equal to 1.2 and 1.3 for a channel 500 feet long is shown in Figure 5.6. For the wave with the discharge ratio $Q_p/Q_b = 1.3$, although the peak depth does become larger over a certain length of channel, it attenuates along the remaining length of channel. While this wave amplifies it does not, however, ever reach the magnitude of its peak depth at the inlet; therefore, it may be classified as an attenuating wave.

Figure 5.7 shows the peak wave depth plot, in a dimensionless form, for the same discharge ratios as in Figure 5.5 except that the time base of the sinusoidal inflow hydrograph has been doubled to 40 seconds. Here again it may be learned that when $\upsilon_p > 1$ a wave amplifies and when $\upsilon_p < 1$ a wave attenuates.

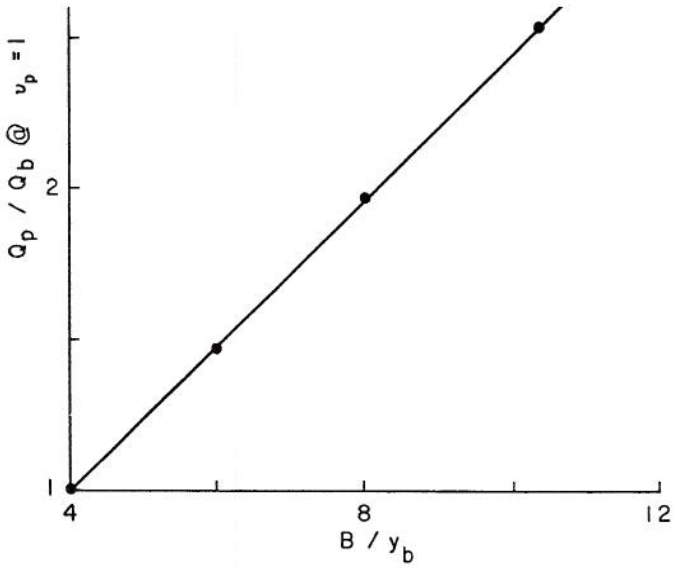

Figure 5.4 Discharge Ratio at which Vedernikov Number is One versus Width-Depth Ratio
$F_b = 3.0$, $y_b = 0.25$, b = 0.0, f = 0.01

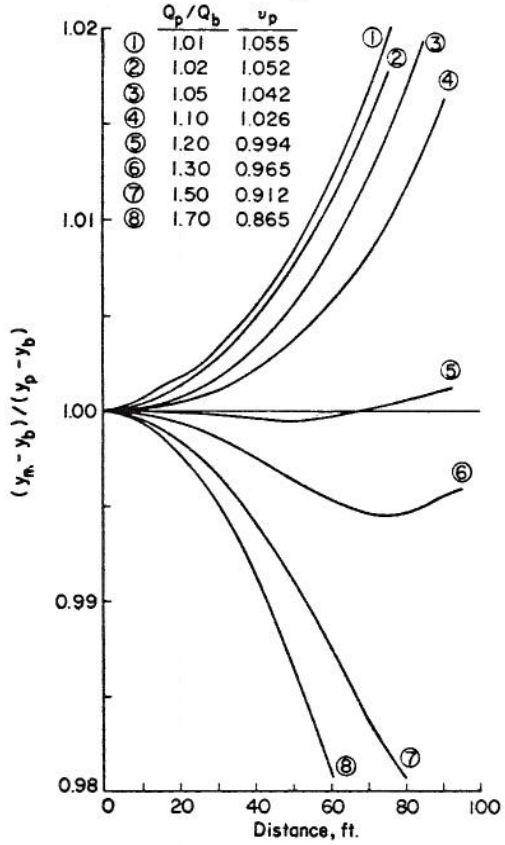

Figure 5.5 Dimensionless Peak Wave Depth versus Distance for 20-Second Duration Sinusoidal Inflow Hydrographs of Various Discharge Ratios
$F_b = 3.0$, $v_b = 1.06$

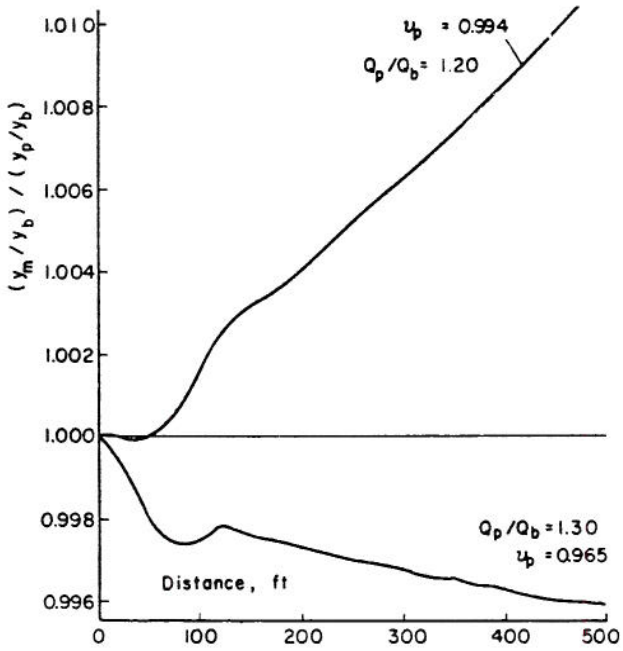

Figure 5.6 Dimensionless Peak Wave Depth versus Distance for 20-Second Duration Sinusoidal Inflow Hydrographs of Various Discharge Ratios
$F_b = 3.0$, $v_b = 1.06$

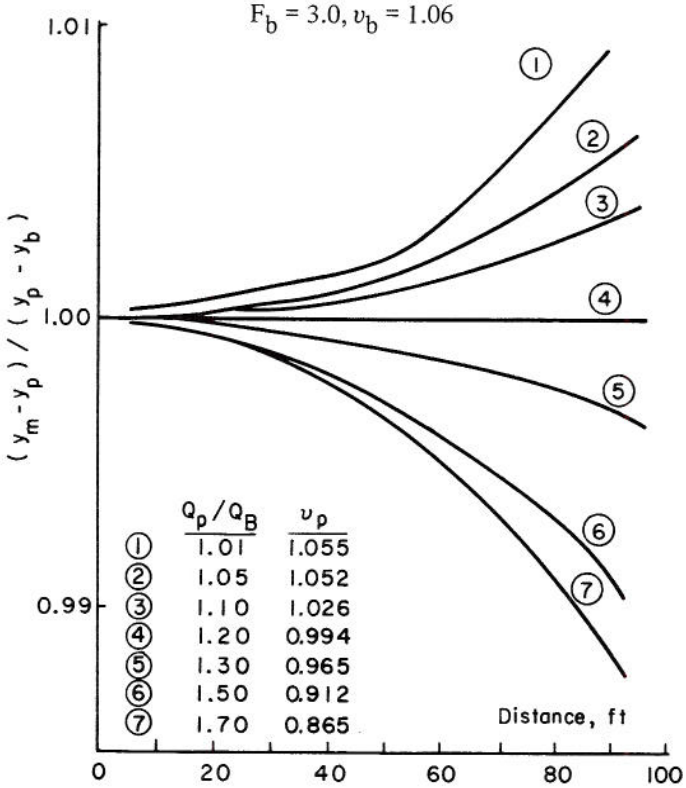

Figure 5.7 Dimensionless Peak Wave Depth versus Distance for a 40-Second Duration Sinusoidal Inflow Hydrograph of Various Discharge Ratios
$F_b = 3.0$, $v_b = 1.06$

By comparing the two graphs it may be seen that the rate of amplification or attenuation varies inversely with the time base of the hydrograph. Also the farther away v_p is from a value of one, the more amplification or attenuation that takes place.

Figures 5.8 and 5.9 show the dimensionless peak wave depth plot for the waves resulting from asymmetric inflow hydrographs shown in Figure 5.1. The results of the advanced peak wave (θ = - 1.0) are shown in Figure 5.8, and those of the retarded peak ($\theta = 0.5$) are shown in Figure 5.9. From both figures it can be seen that the waves amplify when $v_p > 1$ and attenuate when $v_p < 0.96$. Considering the accuracy of numerical simulations, one may say that the waves are neither amplifying nor attenuating when v_p is between 0.97 and 1.00. One may also say that the rate of amplification or attenuation varies with the discharge ratio and the shape of the wave. The above is stated in relative terms, since the plots for physical waves would differ from the above because of the inlet conditions, as explained earlier and shown in Figures 5.2 and 5.3.

The previous plots of dimensionless peak wave depth versus distance had the peak depth Vedernikov number, v_p ,at the inlet as a parameter of each curve. It would be informative to learn whether the peak wave depth Vedernikov number at any distance along the channel remained less than one for an attenuating wave, and greater than one for an amplifying wave. This information is available as may be seen in Figures 5.10, 5.11, and 5.12. Figure 5.10 gives the dimensionless peak wave depth plotted against distance for an attenuating wave in the top portion of the graph. The Vedernikov number is plotted against distance in the bottom position of Figure 5.10. The Vedernikov number remains less than one along the length of the channel; however, it increases in value along the channel length as the peak depth decreases, Figure 5.11, where the Vedernikov number is plotted against distance to 500 feet from the inlet for the same conditions as Figure 5.10. It may be seen that the Vedernikov number of the peak, v_p , never increases to one. Figure 5.12 shows the results for an amplifying wave. The Vedernikov number is always greater than one; and it may decrease in magnitude as the peak depth increases; however, it never attains a value of one.

The results of the findings as discussed above may be summarized in a plot of discharge ratio versus Froude number of base flow as shown in Figure 5.13 for the base flow depth and Chézy resistance law given. The diagonal line divides the graph into two regions. The left one is the attenuation zone, the right zone is the amplification zone. If the flow conditions at the channel inlet are in the left zone, the v_p is less than one, and the wave will attenuate along the channel. If, however, the flow conditions falls in the right zone, the v_p is greater than one, and the wave will amplify along the channel. Along the diagonal line the v_p is equal to one, thereby dividing the plot into amplifying and attenuating regions. For other base flow depths, resistance laws and channel cross sectional shapes, similar graphs can be drawn using the Vedernikov number relation of Chapter 3. This relation also can be used by itself to determine whether a supercritical gradually varied wave resulting from an inflow hydrograph will amplify or attenuate as it travels along a particular channel.

The above shows that the Vedernikov number can be used to determine whether or not a gradually varied, single peaked wave will amplify in a rectangular shaped channel of a particular cross section.

5.4 Some Characteristics of Supercritical Gradually Varied, Single Peaked Waves

The results discussed in this chapter and shown in Figure 5.13 are those of a particular channel size. When the Froude number of the base flow is less than 2.82, the wave will attenuate. When the flow conditions fall in the zone to the right of the diagonal line of Figure 5.13, the wave will amplify. In the former case both the base and peak flow Vedernikov numbers are less than one; in the latter, both the base and peak flow Vedernikov number are greater than one. Although this finding is useful in itself, there are conditions where the base flow Vedernikov number is greater than one, and the peak flow Vedernikov number is less than one. In other words, the bottom portion of the wave is in the right zone, and the top portion of the wave is in the left zone of Figure 5.13. A base flow Froude of 3.0 and a discharge ratio, $Q_p/Q_b = 1.3$, would produce this condition.

Figure 5.14 shows the dimensionless peak wave depth plot for 940 foot long channel with the characteristics described in Section 5.3. The discharge ratio is equal to 1.3 in all three cases. The upper curve where F_b is equal to 4.5 represents an amplifying

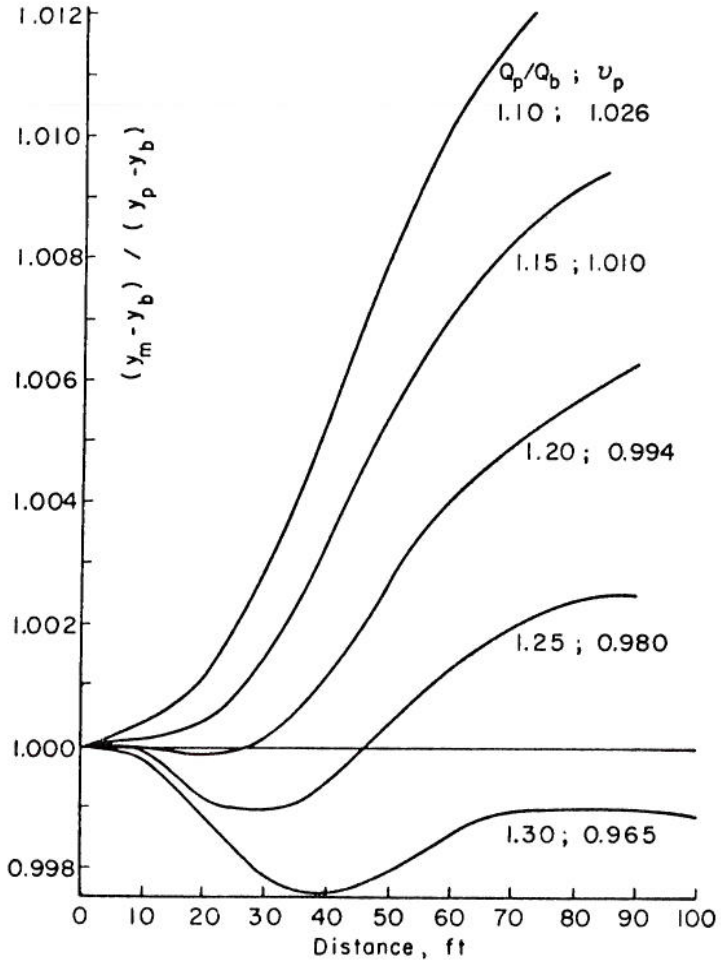

Figure 5.8 Dimensionless Peak Wave Depth versus Distance for Advanced Peak Inflow Hydrographs of Various Discharge Ratios
$F_b = 3.0, v_b = 1.06, \theta = -1.0$

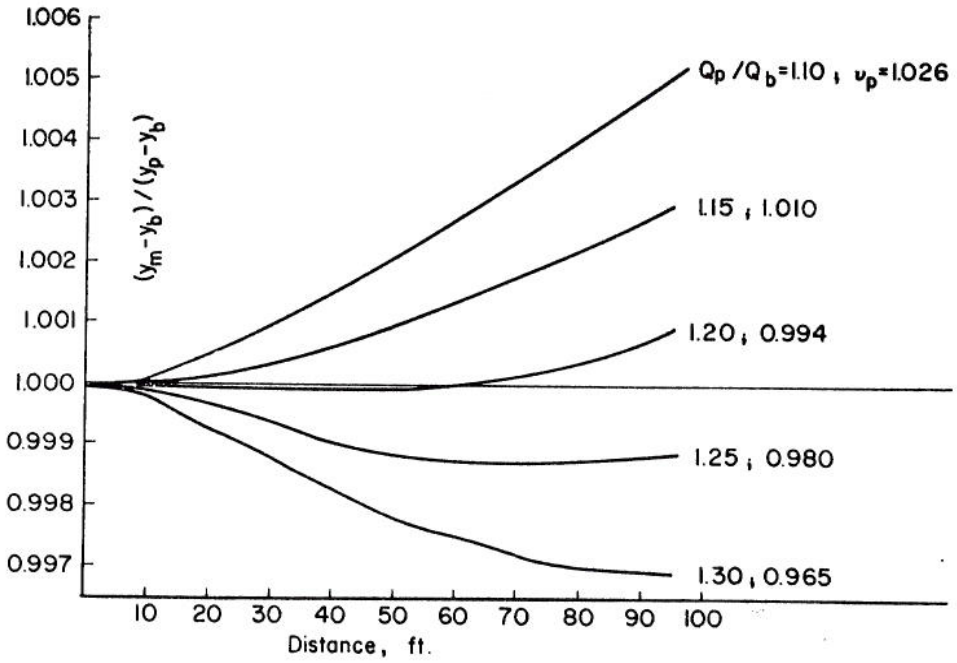

Figure 5.9 Dimensionless Peak Wave Depth versus Distance for Retarded Peak Inflow Hydrographs of Various Discharge Ratios
$F_b = 3.0, v_b = 1.06, \theta = +0.5$

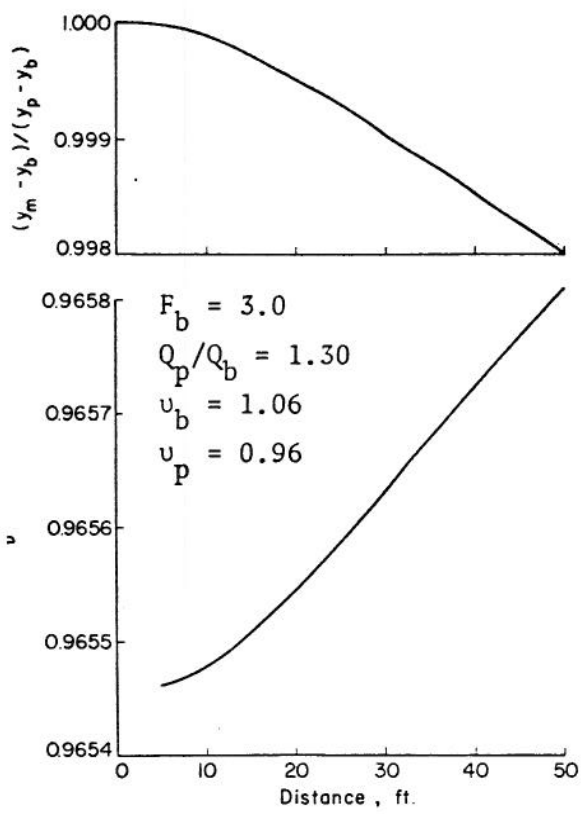

Figure 5.10 Dimensionless Peak Wave Depth and Vedernikov Number versus Distance for an Attenuating Wave

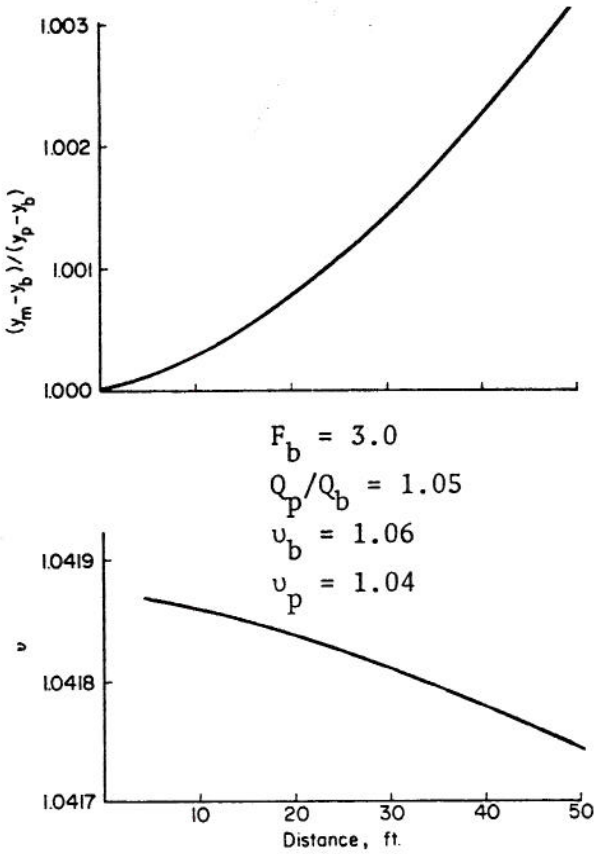

Figure 5.12 Dimensionless Peak Wave Depth and Vedernikov Number versus Distance for an Amplifying Wave

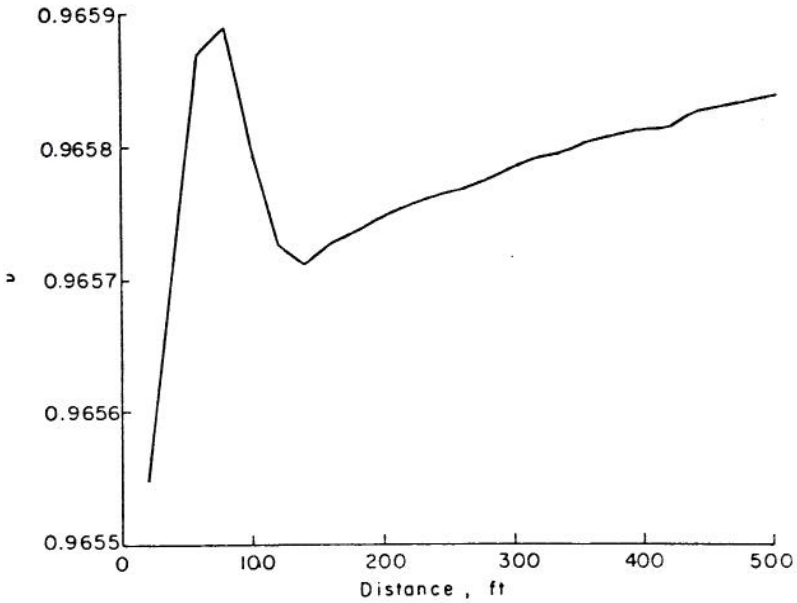

Figure 5.11 Vedernikov Number versus Distance for an Attenuating Wave
F_b = 3.0, Q_p/Q_b = 1.30, υ_b = 1.06, υ_p = 0.96

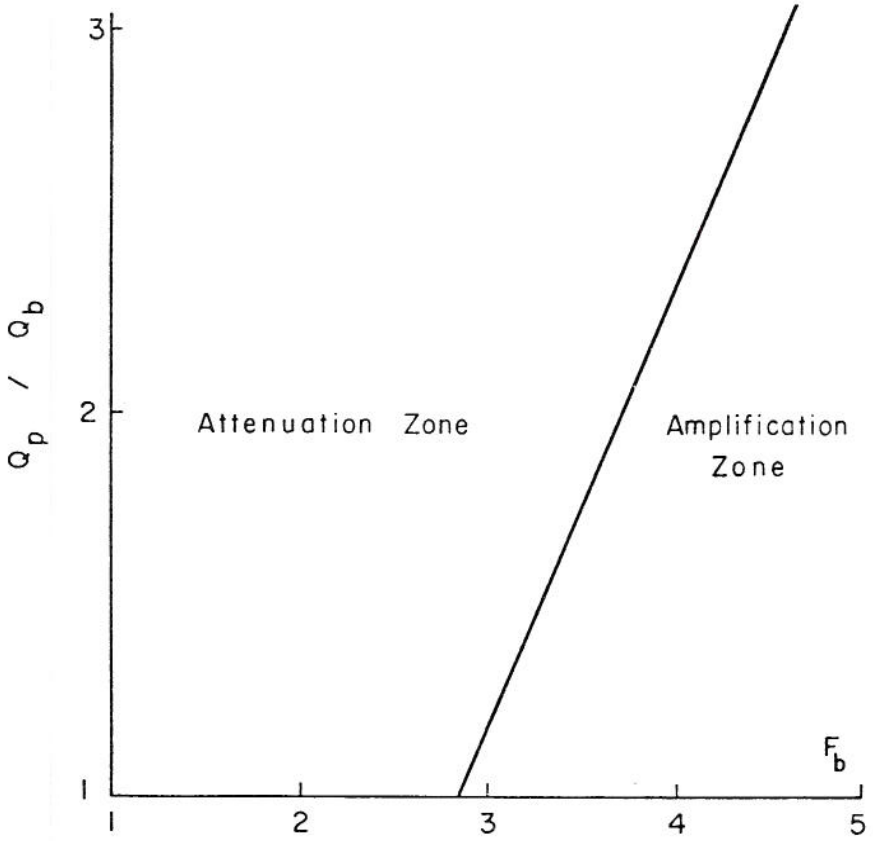

Figure 5.13 Discharge Ratio versus Froude Number of Base Flow
B = 1.2 ft, y_b = 0.25 ft, b = 0.0
f = 0.01

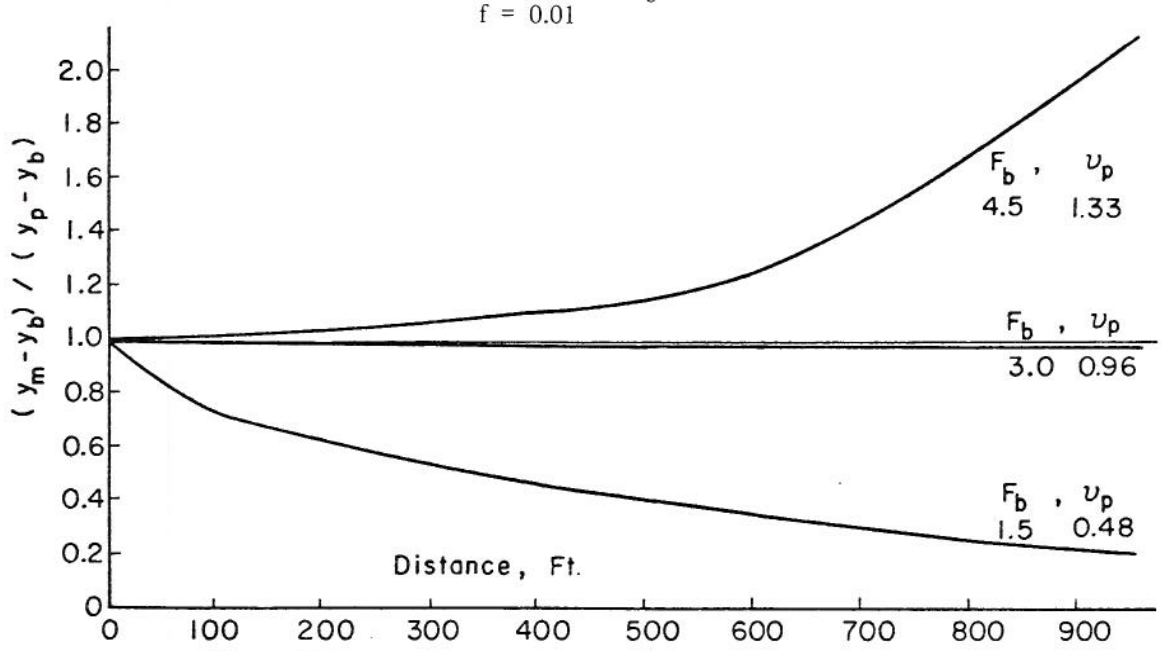

Figure 5.14 Dimensionless Peak Wave Depth versus Distance for Various Base Flow Froude Numbers
Q_p/Q_b = 1.3

wave. The middle curve of F_b equal to 3.0 is mildly attenuating, its peak falls in the attenuating zone, and its base falls in the amplifying zone of Figure 5.13. The lower curve represents an attenuating wave where $F_b = 1.5$.

Figures 5.15, 5.16, and 5.17 show the dimensionless wave depth plotted against time for the three base flow conditions discussed in the previous paragraph at 5, 100 and 200 feet, respectively, along the channel from the inlet. Figure 5.15 shows the attenuating case ($F_b = 1.5$). The peak depth is decreasing and the rear of the wave is flattening with distance. The front of the wave, however, remains relatively constant in shape. Figure 5.16 shows the case for which the base flow Froude number is 3.0 which produces a mildly attenuating condition $v_p = 0.96$. The peak depth decreases as the wave travels along the channel; however, there is little change in the wave shape, but it may be seen that a small negative wave starts to form to the rear of the positive wave. Figure 5.17 shows the case of an amplifying wave ($F_b = 4.5$), where the peak depth becomes larger with distance. A larger negative wave forms on the base flow behind this wave; this negative wave becomes larger with distance travelled along the channel. The rear of the positive wave flattens; however, the degree of flattening is smaller than the wave with the Froude number of the base flow, $F_b = 1.5$.

The different characteristics of attenuating and amplifying waves may also be shown by means of dimensionless depth-discharge relations. Figure 5.18 shows the relations at 45,495 and 975 feet from the inlet for $F_b = 1.5$.

From Figure 5.18 it may be seen that the relation is looped except at the inlet where the normal depth relation is assumed to govern the flow. The rising limb of the wave is to the right of the falling limb, and since $V = f(\Delta Q/\Delta A)$ the velocity of the wave at any given depth is greater on the front than on the rear. This causes the wave to attenuate, since the wave becomes longer and the peak decreases in order to conserve the mass. In Chapter 3 the Seddon celerity is defined by $\partial Q/\partial A$, and the Lagrangian celerity is defined by $V + \sqrt{gy}$. For an attenuating wave the Lagrangian celerity of the front is greater than that of the same depth on the rear. Since the Seddon celerity remains relatively constant on both limbs at the same depth, except in the crest region, the rear of the wave undergoes more distortion than the front for an attenuating wave. The difference in the velocities, and in turn the difference in the celerities, at any relative wave depth increases as the wave travels along the channel. This can be seen in the Figure 5.18 where the loop opens up relative to the height of the loop with the distance travelled. Also time travels around the loop in the counterclockwise direction.

Figure 5.19 shows similar results for the condition where the Froude number of the base flow is 4.5. The depth-discharge relation is again looped; however, the rising and falling depths, as compared to the previous case of Figure 5.18, are on the opposite limbs of the curve. The left side represents the rising limb, the right side the falling limb. These hydraulic conditions produce an amplifying wave, as may be seen in Figures 5.13 and 5.14. At any given wave depth, the velocity on the rear of the wave is greater than on the front. This causes the wave to become shorter and the peak depth increases. In this case, the wave gains mass from the base flow, since a small negative wave forms immediately behind the positive wave as may be seen in Figure 5.17.

The third condition described earlier, *i.e.*, $F_b = 3.0$, produces an attenuating wave. Figure 5.20 shows the depth-discharge relation for this case. Here it may be seen that there is a looped relation for the lower portions of the wave; however, it is difficult to determine from the plot if this is also true for the top portion of the wave. The depth-discharge plot for the peak region of the wave is shown in Figure 5.21. Here it may be seen that the relation is looped, and the larger velocities are on the front. On the bottom portion of the wave the opposite is true: the larger velocities are on the rear. Therefore if the depth-discharge relation was plotted on a very large plot, a curve in the form of a figure eight would be seen. Time would pass around the lower portion in a clockwise direction, similar to an amplifying wave; it would pass around the top portion in a counter-clockwise direction, similar to an attenuating wave. The relative depth where the two loops meet is 0.57 which represents approximately the discharge ratio Q/Q_p, at which a F_b of 3.0 will neither attenuate nor amplify as shown in Figure 5.13.

Figure 5.22 shows the ratio of velocity on the rear, V_r, to the velocity on the front, V_f, hereafter called the velocity ratio, of a wave at any given depth plotted against wave depth for the case where $F_b = 3.0$. As explained earlier, the top portion of an

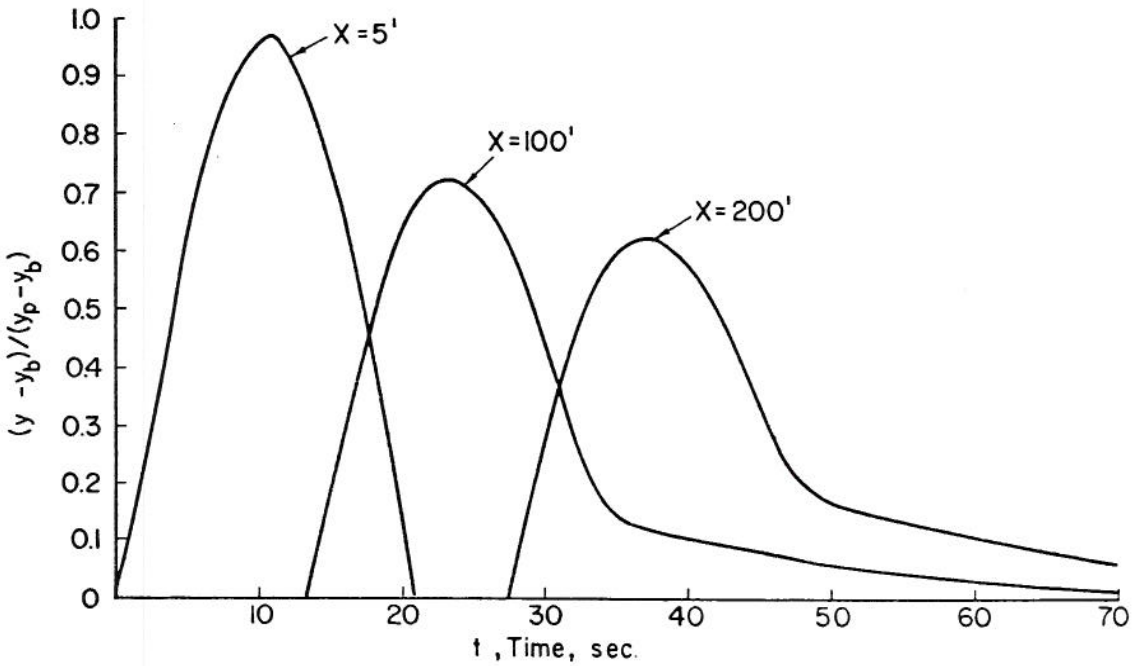

Figure 5.15 Dimensionless Wave Depth Hydrographs for an Attenuating Wave $F_b = 1.5$, $Q_p/Q_b = 1.3$, $v_b = 0.53$, $v_p = 0.48$

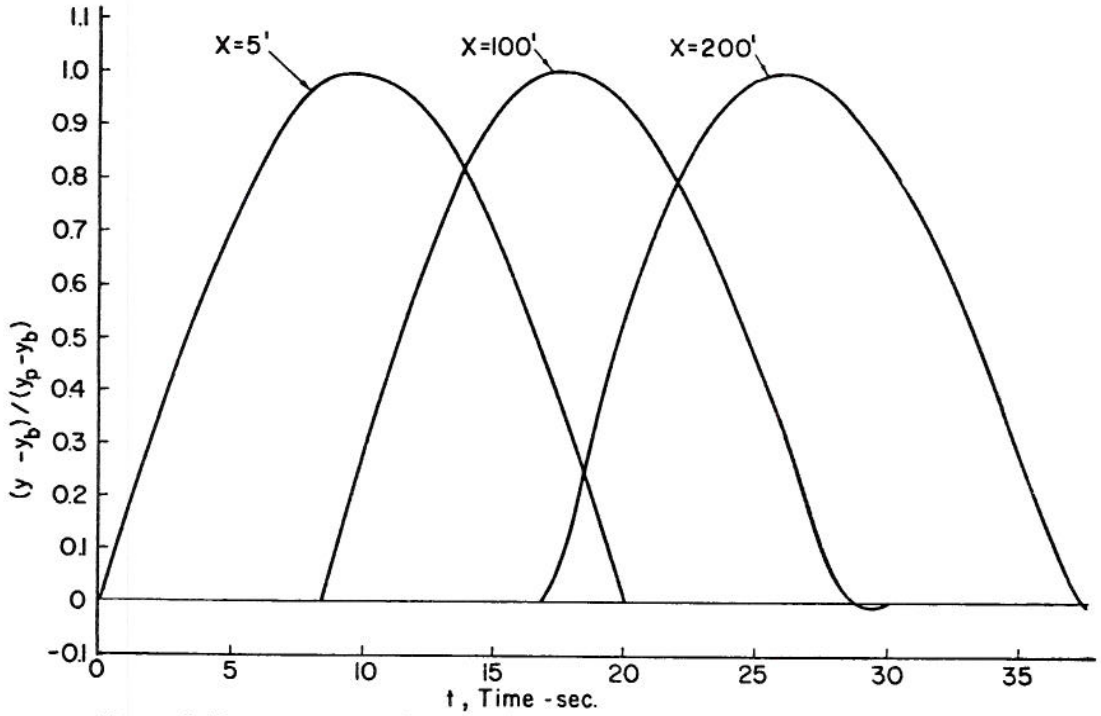

Figure 5.16 Dimensionless Wave Depth Hydrographs for a Mildly Attenuating Wave $F_b = 3.0$, $Q_p/Q_b = 1.3$, $v_b = 1.06$, $v_p = 0.96$

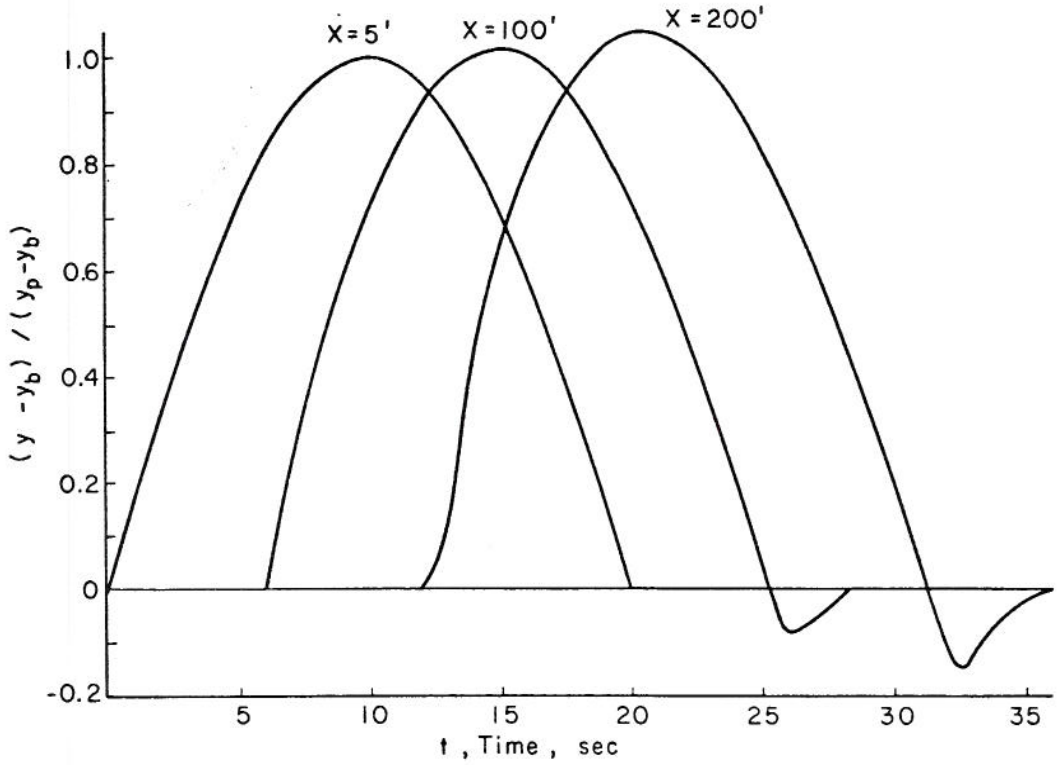

Figure 5.17 Dimensionless Wave Depth Hydrographs for an Amplifying Wave
F_b = 4.5, Q_p/Q_b = 1.3, v_b = 1.36, v_p = 1.33

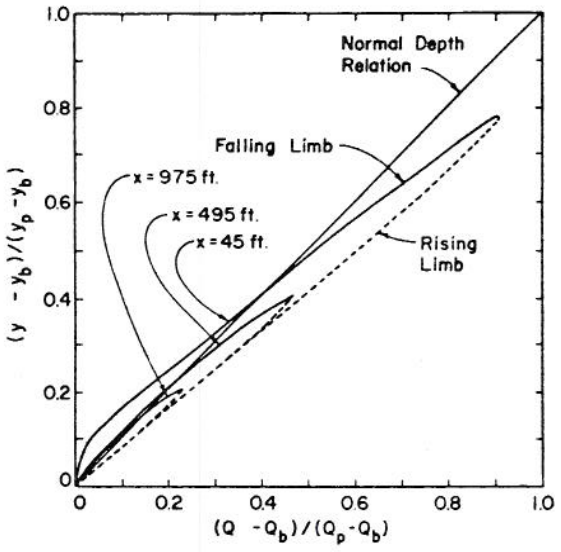

Figure 5.18 Dimensionless Wave Depth versus Discharge Plot for an Attenuating Wave
F_b = 1.5, Q_p/Q_b = 1.3, v_b = 0.53, v_p = 0.48

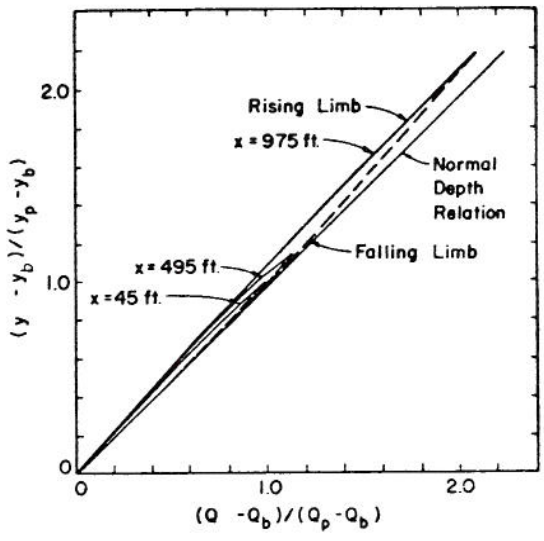

Figure 5.19 Dimensionless Wave Depth versus Discharge Plot for an Amplifying Wave
F_b = 4.5 Q_p/Q_b = 1.3, v_b = 1.36, v_p = 1.33

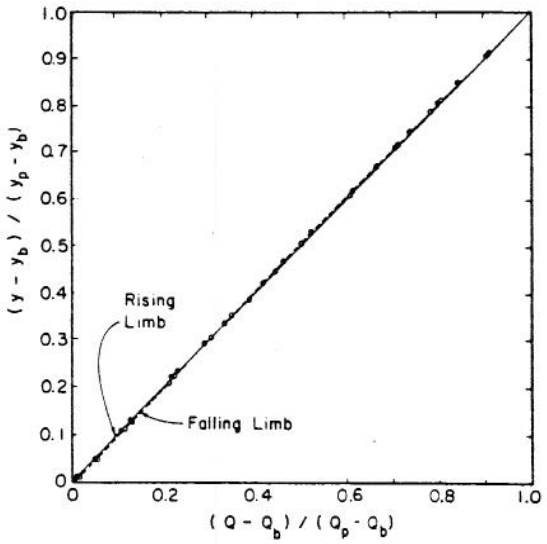

Figure 5.20 Dimensionless Wave Depth versus Discharge Plot for a Mildly Attenuating Wave
F_b = 3.0, Q_p/Q_b = 1.30, υ_b = 1.06, υ_p = 0.96

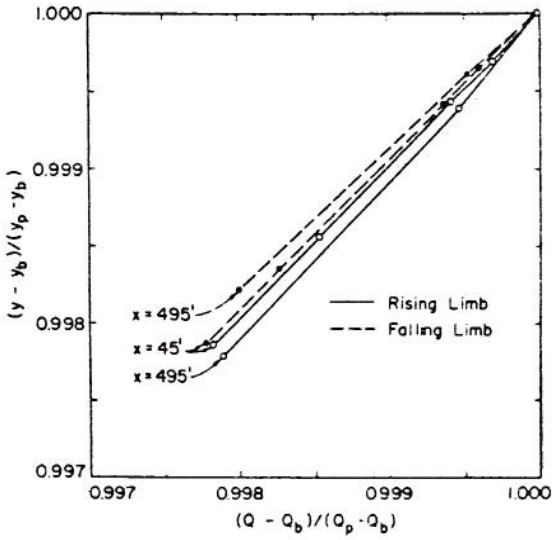

Figure 5.21 Dimensionless Wave Depth versus Discharge Plot for the Crest of a Mildly Attenuating Wave.
F_b = 3.0, Q_p/Q_b = 1.30, υ_b = 1.06, υ_p = 0.96

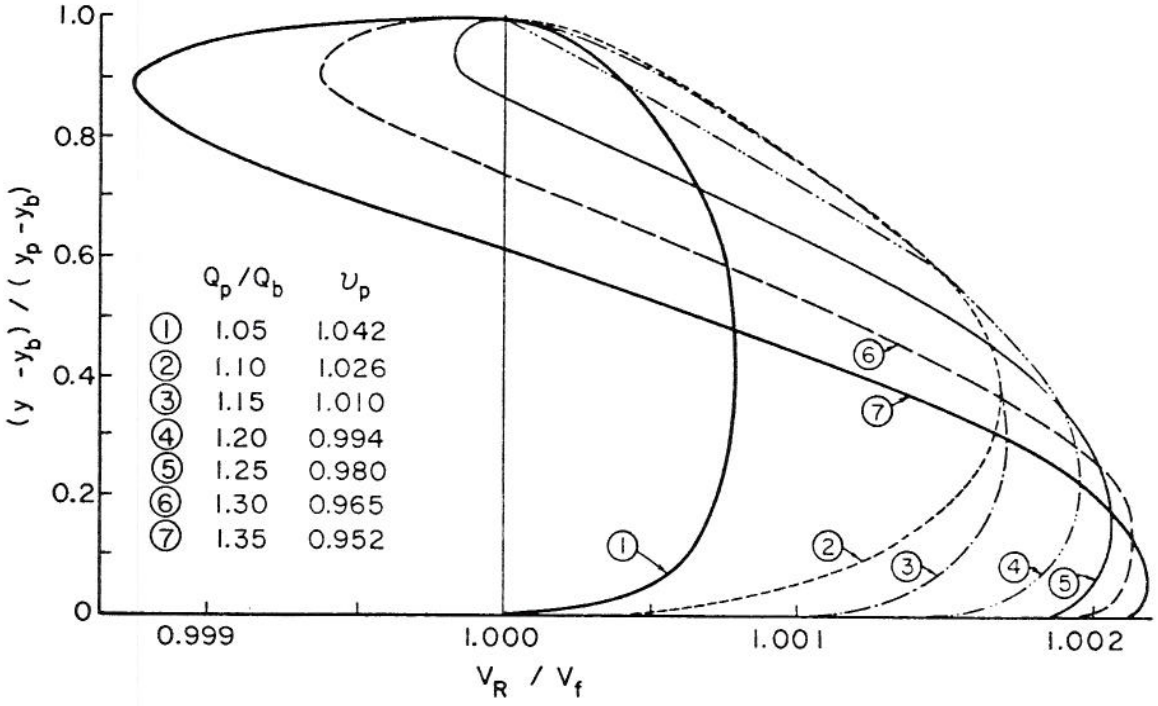

Figure 5.22 Velocity Ratio versus Wave Depth for Various Discharge Ratios
F_b = 3.0, υ_b = 1.06

attenuating wave will have the velocity ratios less than one, and an amplifying wave will have the ratios greater than one. From this graph it may be seen that when the Vedernikov number of the inlet peak, v_p is greater than one then the velocity ratios are greater than one over the wave depth. When v_p is less than one, the V_r/V_f are greater than one for the lower portion of the wave, but less than one for the top portion. The wave depth at which the velocity ratio equal to one corresponds to the point where the two loops meet in the corresponding depth-discharge plot. The wave depth for $V_r/V_f = 1$ decreases as v_p decreases, as can be seen from the position where the curves cross the vertical line representing a velocity ratio of one. The same property can be observed in Figure 5.23 where Q_p/Q_b, and indirectly v_p, is plotted against the dimensionless wave depth. When $Q_p/Q_b = 1.20$ then $V_r/V_f = 1$ for $y = y_p$. It may be seen that as Q_p/Q_b increases the Vedernikov number at the peak, v_p thereby decreases, and the position where $V_r/V_f = 1$, moves down the wave profile. At a higher base flow Froude number, *i.e.*, $F_b = 4.5$, the velocity ratio is greater than one over the whole wave profile and the time travels around the depth-discharge loop clockwise.

Some properties of a wave crest whose hydraulic conditions are near the diagonal line in Figure 5.13 can be seen in Figure 5.24, where $(Q-Q_b)/(Q_p-Q_b)$ is plotted against

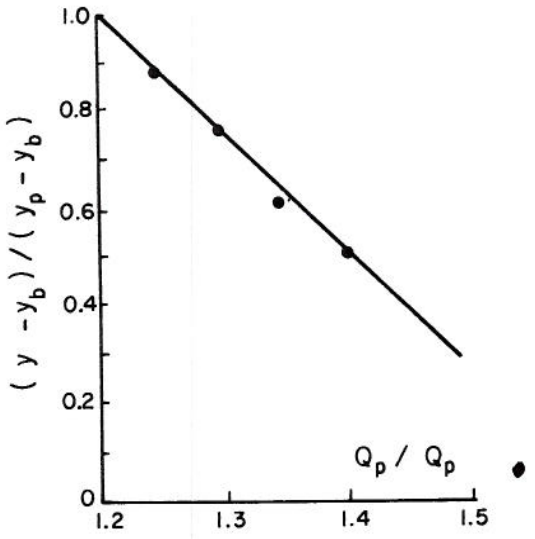

Figure 5.23 Wave Depth where Velocity Ratio is Equal to One versus Discharge Ratio $F_b = 3.0, v_b = 1.06$

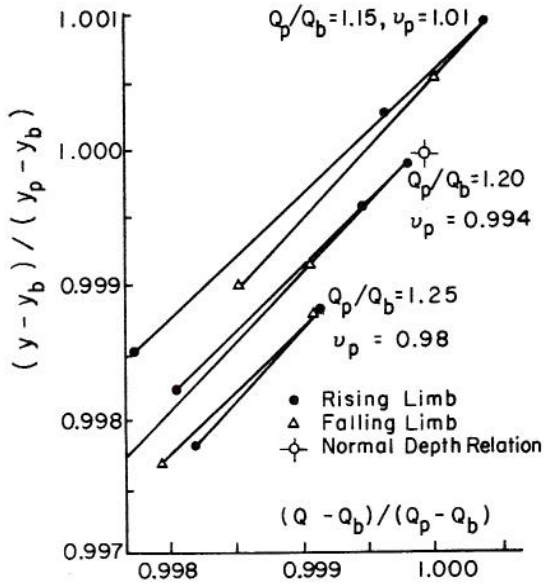

Figure 5.24 Dimensionless Wave Depth versus Discharge Plot at the Crest of the Wave for Various Discharge Ratios $F_b = 3.0, v_b = 1.06$

$(y-y_b)/(y_p-y_b)$ in which Q_p and y_p are the peak discharge and depth, respectively, at the inlet. The base flow Froude number is equal to 3.0 which is the intermediate value of those discussed earlier. Therefore, when $(y-y_b)/(y_p-y_b)$ is greater than one, the wave is amplifying; when $(y-y_b)/(y_p-y_b)$ is equal to one, the wave is neither amplifying nor attenuating; and when $(y-y_b)/(y_p-y_b)$ is less than one, the wave is attenuating. From the plot it may be seen that when $v_p = 1.01$ the wave is amplifying, and the velocities on the rear of the crest are larger than on the front. When $v_p = 0.98$ the wave is attenuating, and the velocities on the front of the crest are greater than on the rear. The middle curve in the plot is for the resulting wave from an inflow hydrograph for which $v_p = 0.994$. The lower portion of the loop would indicate that the velocity at a given depth on the rear of the crest is greater than at the same depth on the front of the crest, as can be seen in Figure 5.22. At the peak, however, there is very little difference between the velocites at any given depth as may be seen in Figure 5.24.

The above results, where Q_p/Q_b is varied while keeping the base flow Froude number constant, confirms the results of the influences of velocities on the front and rear of the wave; it also confirms the shapes of the depth-discharge relation for both attenuating and amplifying waves, which were determined earlier by holding Q_p/Q_b constant and varying the base flow Froude number.

Chapter 6

CONCLUSIONS

Gradually varied, single peaked waves flowing with supercritical velocities in a rectangular channel were simulated by applying the specified intervals scheme of the method of characteristics solution to the governing equations. Thus, numerical analysis replaced physical experimentation which would be expensive to conduct and from which accurate results would be difficult to obtain without significant effort. From the analysis of the accelerations on the wave crests, it is found, in general, that the waves studied were gradually varied in that the vertical accelerations were negligible.

From this study it was found that the Vedernikov number can not only be used to determine whether or not roll waves will form on uniform flow, but also whether gradually varied, single peaked waves will amplify or not. When the Vedernikov number of a wave peak is less than one, the wave will attenuate; when the Vedernikov number of a wave peak is greater than one, the wave will amplify. If the Vedernikov number of a wave peak is greater than one, and if the channel is long enough, the front of a wave will continue to steepen and eventually become a bore.

Some hydraulic properties of gradually varied, single peaked waves found are as follows.

(1) The velocities at a given depth either on the top portion or over the total wave profile are greater on the front than on the rear of an attenuating wave.

(2) The velocities at a given depth are greater on the rear than on the front of an amplifying wave.

(3) With an attenuating wave time travels around the looped depth-discharge relation in a counterclockwise direction.

(4) With an amplifying wave, time travels around the looped depth-discharge relation in a clockwise direction.

In the supercritical regime, gradually varied waves may be classified into three types that are dependent on the Vedernikov number of the flow:

(a) when the Vedernikov number is less than one over the wave profile, the wave is attenuating;

(b) when the Vedernikov number is less than one on the top portion of the wave profile and greater than one on the bottom portion, the wave is attenuating, and

(c) when the Vedernikov number is greater than one over the wave profile, the wave is amplifying.

REFERENCES

Abbott, M. M., An Introduction to the Method of Characteristics, American Elsevier, New York, 1966.

Ackers, P., and Harrison, A. J. M., Attenuation of Flood Waves in Part-Full Pipes, Proceedings, Institution of Civil Engineers, Vol. 29, July 1964.

Blair, J., High Bridge to Paradise, Highway Magazine, September 1961.

Brock, R. R., Development of Roll Waves in Open Channels, Report No. KH-R-16, W. M. Keck Laboratory of Hydraulics and Water Resources, California Institute of Technology, Pasadena, California, July 1967.

Brock, R. R., Periodic Roll Waves, Journal of Hydraulics Division, ASCE, Vol. 98, HY12, December 1970.

Chow, V. T., Open Channel Hydraulics, McGraw-Hill, New York, 1959.

Courant, R. R. Friedricks, K. O., Supersonic Flow and Shock Waves, Interscience Publishers, New York, 1948.

Crandall, Engineering Analysis: A Survey of Numerical Procedures, McGraw Hill, New York, 1956.

Craya, A., The Criterion for the Possibility of Roll-Wave Formation in Inclined Open Channels, National Bureau of Standards Circular – 521, Washington, D.C., 1952.

Dressler, R. F., Mathematical Solution of the Problem of Roll-Waves in Inclined Open Channels, Communications on Pure and Applied Mathematics, Vol. 2, 1949.

Dressler, R. F., Stability of Uniform Flow and Roll-Wave Formation in Gravity Waves, National Bureau of Standards, Circular 521, Washington, D.C., 1952.

Dressler, R. F., and Pohve, F. V., Resistance Effects on Hydraulic Instability, Communications on Pure and Applied Mathematics, Vol. 6, 1953, pp. 93-96.

Escoffier, F. F., A Graphical Method for Investigating the Stability of Flow in Open Channels or in Closed Conduits Flowing Full, Trans. A.G.U., Vol. 31, No. 4, August 1950.

Excoffier, F. F., and Boyd, M. B., Stability Aspects of Flow in Open Channels, Journal of Hydraulics Division, ASCE, Vol. 88, HY6, November 1962.

Ghambarian, H. H., On Waves in Inclined Open Channels, IAHR 11th International Congress, Leningrad, 1965, Vol. 1 (1.1) 1965, pp. 1-10.

Henderson, F. M., Open Channel Flow, Macmillan Co., New York, 1966.

Holmes, W. H., Traveling Waves in Steep Channels, Civil Engineering Vol. 6, No. 7, 1936.

Iwagaki, Y., On the Laws of Resistance to Turbulent Flow in Open Smooth Channels, Proceedings of the 2nd Japan National Congress for Applied Mech., 1952.

Iwagaki, Y., On the Laws of Resistance to Turbulent Flow in Open Rough Channels, Proceedings of the 4th Japan National Congress for Applied Mech., 1954.

Iwasa, Y., The Criterion for Instability of Steady Uniform Flows in Open Channels, Kyoto Univeristy, Faculty Mem. Vol. 16, pp. 264-275.

Kewlegan, G. H., and Patterson, G. H., Effect of Turbulence and Channel Slope on Translation Waves, Journal of Research of the National Bureau of Standards, Vol. 20, June 1943.

Kewlegan, G. H., and Patterson, G. W., A Criterion for Instability of flow in Steep Channels, Trans. A.G.U., Vol. 21, 1970.

Koloseus, H. J., The Effect of Free-Surface Instability on Channel Resistance, Ph.D. Thesis, State University of Iowa, 1958.

Koloseus, H. J., and Davidian J., Free-Surface Instability Correlations, United States Geological Survey Water-Supply Paper 1599-C, 1966.

Liggett, J. A. and Woolhiser, D. A., Difference Solutions of the Shallow-Water Equations, Journal of the Engineering Mechanics Division, ASCE, Vol. 93, No. EM2, April 1967.

Massau, J., Appendice au Memorie sur l'Integration Graphique, Assoc. des Ingenieus Sortis des Ecoles Speciales de Grand (Belgium) Annales Vol. 12, 1889.

Mayer, P. G., Roll Waves and Slug Flows in Inclined Open Channels, Journal of the Hydraulic Division, ASCE, Vol. 85, HY7, Proceedings Paper 2085, July 1959.

Pinkayan, S. and Barnes, A. H., Unsteady Free-Surface Flow in a Storm Drain in Lateral Inflows, Report for U.S. Bureau of Public Roads, Engineering Research Center, Colorado State University, 1967.

Salvadori, M. G. and Baron, M. L., Numerical Methods in Engineering, Prentice-Hall, Englewood Cliffs, N. J., 1961.

Southworth, R. W., and Deleeuiv, S. L., Digital Computation and Numerical Methods, McGraw Hill, New York, 1965.

Stoker, J. J., Water Waves – The Mathematical Theory with Application, Interscience, New York, 1957.

Streeter, V. L. and Wylie, E. B., Hydraulic Transients, McGraw-Hill, New York, 1967.

Thomas, H. A., The Propogation of Waves in Steep Prismatic Conduits, Proceedings of the Hydraulic Conference, Iowa City, Iowa, 1940.

Vedernikov, V. V., Conditions at the Front of a Translation Wave Distributing a Steady Motion of a Real Field, C. R. (Doklady), Academy of Science U.S.S.R., Vol. 48, No. 4, 1945.

Vedernikov, V. V., Characteristic Features of a Liquid Flow in an Open Channel, C. R. (Doklady), Academy of Science U.S.S.R., Vol. 52, 1946.

Watson, W. A., Philipson, T. and Oates, P. J., Numerical Analysis, Vol. 2, American Elsevier, New York, 1969.

Wylie, E. B., Unsteady Free-Surface Flow Computations Journal of Hydraulic Division, ASCE, Vol. 96, HY11, November 1970.

Yevjevich, V. M., Bibliography and Discussion of Flood-Routing Methods and Unsteady Flow in Channels, United States Geological Survey Water-Supply Paper 1690, Washington, 1964.

Yevjevich, V. M., Rate of Change of the Peak for Floods Progressing Along a Channel, IAHR 11th International Congress, Leningrad, September 7-11, 1965, La HB No. 5, p. 419.

Yevjevich, V. M., and Barnes, A. H., Flood Routing Through Storm Drains – Part I. Solution of Problems of Unsteady Free-Surface Flow in Storm Drains, Hydrology Paper No. 43, Colorado State University, Fort Collins, Colorado, November 1970.

Yevjevich, V. M., and Barnes, A. H., Flood Routing Through Storm Drains – Part IV. Numerical Computer Methods of Solution, Hydrology Paper No. 46, Colorado State University, Fort Collins, Colorado, November 1970.

Zovne, J. J., The Numerical Solution of Transient Supercritical Flow by the Method of Characteristics with Technique for Simulating Bore Propagation, ERC-0370 School of Civil Engineering, Georgia Institute of Technology, May 1970.

KEY WORDS: Open Channels, Supercritical, Gradually Varied Flow, Method of Characteristics, Specified Intervals Scheme, Integration Techniques, Amplification Criterion.

ABSTRACT: Some hydraulic properties, obtained using the Chezy resistance law, that distinguish amplifying waves from attenuating waves are found by a numerical integration of the governing hyperbolic, partial differential equations of supercritical, gradually varied waves flowing in a channel with a rectangular cross section. The supercritical, gradually varied flow is simulated by using various integration techniques of the specified intervals scheme of the method of characteristics solution to the governing system of equations. One of these integration techniques is used to determine attenuation and amplification characteristics of gradually varied, single peaked waves. Prior to this determination, criteria found by various investigators for predicting the stability of uniform flow

KEY WORDS: Open Channels, Supercritical, Gradually Varied Flow, Method of Characteristics, Specified Intervals Scheme, Integration Techniques, Amplification Criterion.

ABSTRACT: Some hydraulic properties, obtained using the Chezy resistance law, that distinguish amplifying waves from attenuating waves are found by a numerical integration of the governing hyperbolic, partial differential equations of supercritical, gradually varied waves flowing in a channel with a rectangular cross section. The supercritical, gradually varied flow is simulated by using various integration techniques of the specified intervals scheme of the method of characteristics solution to the governing system of equations. One of these integration techniques is used to determine attenuation and amplification characteristics of gradually varied, single peaked waves. Prior to this determination, criteria found by various investigators for predicting the stability of uniform flow

KEY WORDS: Open Channels, Supercritical, Gradually Varied Flow, Method of Characteristics, Specified Intervals Scheme, Integration Techniques, Amplification Criterion.

ABSTRACT: Some hydraulic properties, obtained using the Chezy resistance law, that distinguish amplifying waves from attenuating waves are found by a numerical integration of the governing hyperbolic, partial differential equations of supercritical, gradually varied waves flowing in a channel with a rectangular cross section. The supercritical, gradually varied flow is simulated by using various integration techniques of the specified intervals scheme of the method of characteristics solution to the governing system of equations. One of these integration techniques is used to determine attenuation and amplification characteristics of gradually varied, single peaked waves. Prior to this determination, criteria found by various investigators for predicting the stability of uniform flow

are shown to be equivalent. One of the criteria, the Vedernikov number, which contains parameters dependent on the frictional law, channel cross-sectional shape and Froude number, is also the criterion for predicting amplification of gradually varied, single peaked waves.

REFERENCE: Jolly, John Peter and Vujica Yevjevich, Colorado State University, Hydrology Paper No. 51 (December, 1971) "Amplification Criterion of Gradually varied, single peaked Waves".

are shown to be equivalent. One of the criteria, the Vedernikov number, which contains parameters dependent on the frictional law, channel cross-sectional shape and Froude number, is also the criterion for predicting amplification of gradually varied, single peaked waves.

REFERENCE: Jolly, John Peter and Vujica Yevjevich, Colorado State University, Hydrology Paper No. 51 (December, 1971) "Amplification Criterion of Gradually varied, single peaked Waves".

are shown to be equivalent. One of the criteria, the Vedernikov number, which contains parameters dependent on the frictional law, channel cross-sectional shape and Froude number, is also the criterion for predicting amplification of gradually varied, single peaked waves.

REFERENCE: Jolly, John Peter and Vujica Yevjevich, Colorado State University, Hydrology Paper No. 51 (December, 1971) "Amplification Criterion of Gradually varied, single peaked Waves".

are shown to be equivalent. One of the criteria, the Vedernikov number, which contains parameters dependent on the frictional law, channel cross-sectional shape and Froude number, is also the criterion for predicting amplification of gradually varied, single peaked waves.

REFERENCE: Jolly, John Peter and Vujica Yevjevich, Colorado State University, Hydrology Paper No. 51 (December, 1971) "Amplification Criterion of Gradually varied, single peaked Waves".

LIST OF 25 HYDROLOGY PAPERS CONTAINED IN VOLUME NO. I

LIST OF 25 PAPERS CONTAINED IN VOLUME NO. II

No. 26 The Investigation of Relationship Between Hydrologic Time Series, and Sunspot Numbers, by Ignacio Rodrigues-Iturbe and Vujica Yevjevich, April 1968.

No. 27 Diffusion of Entrapped Gas from Porous Media, by Kenneth M. Adam and Arthur T. Corey, April 1968.

No. 28 Sampling Bacteria in a Mountain Stream, by Samuel H. Kunkle and James R. Meiman, March 1968.

No. 29 Estimating Design Floods from Extreme Rainfall, by Frederick C. Bell, July 1968.

No. 30 Conservation of Soil Water by Gravel Mulches, A. T. Corey and W. K. Kemper, September 1968.

No. 31 Effects of Truncation on Dependence in Hydrological Time Series, by Rezaul Karim Bhuiya and Vujica Yevjevich, November 1968.

No. 32 Properties of Non-Homogeneous Hydrologic Series, by V. Yevjevich and R. I. Jeng, April 1969.

No. 33 Runs of Precipitation Series, by Jose Llamas and M. M. Siddiqui, May 1969.

No. 34 Statistical Discrimination of Change in Daily Runoff, by Andre J. Dumas and Hubert J. Morel-Seytoux, August 1969.

No. 35 Stochastic Process of Precipitation, by P. Todorovic and V. Yevjevich, September 1969.

No. 36 Suitability of the Upper Colorado River Basin for Precipitation Management, by Hiroshi Nakamichi and H. J. Morel-Seytoux, October 1969.

No. 37 Regional Discrimination of Change in Runoff, by Viboon Nimmanit and Hubert J. Morel-Seytoux, November 1969.

No. 38 Evaluation of the Effect of Impoundment on Water Quality in Cheney Reservoir, by J. C. Ward and S. Karaki, March 1970.

No. 39 The Kinematic Cascade as a Hydrologic Model, by David F. Kibler and David A. Woolhiser, February 1970.

No. 40 Application of Run-Lengths to Hydrologic Series, by Jaime Saldarriaga and Vujica Yevjevich, April 1970.

No. 41 Numerical Simulation of Dispersion in Groundwater Aquifers, by Donald Lee Reddell and Daniel K. Sunada, June 1970.

No. 42 Theoretical Probability Distribution for Flood Peaks, by Emir Zelenhasic, December 1970.

No. 43 Flood Routing Through Storm Drains, Part I, Solution of Problems of Unsteady Free Surface Flow in a Storm Drain, by V. Yevjevich and A. H. Barnes, November 1970.

No. 44 Flood Routing Through Storm Drains, Part II, Physical Facilities and Experiments, by V. Yevjevich and A. H. Barnes, November 1970.

No. 45 Flood Routing Through Storm Drains, Part III, Evaluation of Geometric and Hydraulic Parameters, by V. Yevjevich and A. H. Barnes, November 1970.

No. 46 Flood Routing Through Storm Drains, Part IV, Numerical Computer Methods of Solution, by V. Yevjevich and A. H. Barnes, November 1970.

No. 47 Mathematical Simulation of Infiltrating Watersheds, by Roger E. Smith and David A. Woolhiser, January 1971.

No. 48 Models for Subsurface Drainage, by W. E. Hedstrom, A. T. Corey and H. R. Duke, February 1971.

No. 49 Infiltration Affected by Flow of Air, by David B. McWhorter, May 1971.

No. 50 Probabilities of Observed Droughts, by Jaime Millan and Vujica Yevjevich, June 1971.